

# Mineralogy and geochemistry of fine-grained clastic rocks in the Eocene Huadian Basin (NE China): Implications for sediment provenance, paleoclimate and depositional environment

QingTao MENG<sup>1,2,✉</sup>, Reinhard F. SACHSENHOFER<sup>2</sup>, ZhaoJun LIU<sup>1</sup>, PingChang SUN<sup>1</sup>, Fei HU<sup>1</sup>, RenJie ZHOU<sup>3</sup> & KeBing WANG<sup>1</sup>

<sup>1</sup> College of Earth Sciences, Jilin University, 130061 Changchun, China;

<sup>2</sup> Department Applied Geosciences and Geophysics, Montanuniversität, 8700 Leoben, Austria;

<sup>3</sup> School of Earth and Environmental Sciences, The University of Queensland, St Lucia, 4072 QLD, Australia;

<sup>✉</sup> Corresponding author, mengqt@jlu.edu.cn

**KEYWORDS** Fine-grained sediments; Oil Shale; Geochemistry; Provenance; Paleoclimate; Environment; Huadian Basin

## Abstract

The Huadian Basin is a small fault-controlled basin in northeast China. It is filled by the Eocene Huadian Formation comprising thick lacustrine oil shale-and coal-bearing sediments. Oil shale, mudstone and carbonaceous shale samples have been collected to determine their mineralogical and geochemical (major, trace and rare earth elements) characteristics. These data are used to evaluate sediment provenance as well as paleoclimate and depositional environment. The fine-grained sediments in the Huadian Formation are derived from felsic volcanic rocks and granites, mixed with minor amounts of mafic and sedimentary rocks. Geochemical proxies confirm sediment recycling in the source region. Clay mineralogy and indices of chemical alteration suggest that a subtropical warm and humid climate prevailed during deposition of the fine-grained sediments. The data also suggest climatic changes during deposition of the Huadian Formation, from a stable warm and humid climate causing intermediate chemical weathering (Pyrite Member), to a seasonal dry-wet climate (Oil Shale Member), to a stable warmer and more humid climate causing strong chemical weathering (Carbonaceous Shale Member). Based on inorganic proxies, the fine-grained sediments in the Huadian Formation have been deposited in an anoxic fresh-water environment. Only the sediments of the Oil Shale Member reflect fluctuating freshwater and brackish conditions. The Eocene climatic change controlled lake level variations and water chemistry. A brackish and strictly anoxic environment together with a warm and humid climate was beneficial for the formation of high quality oil shale, whereas fresh-water conditions and warm and more humid climate favored peat accumulation.

## 1. Introduction

The inorganic geochemistry of lacustrine fine-grained sediments, including oil shale has been used effectively to evaluate depositional environments, paleoclimate and weathering conditions (Chamley 1980; Last and Smol, 2001; Charles et al., 2008; Chen et al., 2003; Jin et al., 2006; Goldberg and Humayun, 2010; Laird et al., 2003; Meng et al., 2012; Bai et al., 2015). Because of different geochemical behaviors during weathering, sediment transport and deposition, some major, trace and rare earth elements (REEs) are useful indicators of sedimentary provenance and sedimentary processes. For example, an increase in the degree of weathering is accompanied by a decrease in concentrations of CaO, K<sub>2</sub>O, Na<sub>2</sub>O and an enrichment of Al<sub>2</sub>O<sub>3</sub>. Some trace elements (e.g. Ni, V, Cr) are sensitive to redox conditions. REEs, Th and Sc as well as other elements (U, Rb) are least fractionated by various sedimentary process (Taylor and McLennan, 1985; McLennan, 1989, 1993, 2001; Johnsson, 1993; Das and Haake 2003; Weltje and von Eynatten, 2004; Jin et al., 2006; Bai et al., 2015; Li et al., 2017).

The Huadian Basin, located in northeastern China (Fig.1a), is filled by Eocene lacustrine sediments (Meng et al., 2011, 2012b; Sun et al., 2013). Together with the Fushun and Meihe Basins, the Huadian Basin is located along the Dunhua-Mishan Fault Zone (Fig.1b). A high number of oil shale and coal layers are mined underground in the Huadian Basin. Although the oil

shale layers are typically only a few meters thick, the oil yield is very high and reaches 24.8%, which is considered amongst the highest oil yields in China. The extensive, high quality oil shale and coal deposits in the Eocene Huadian Formation have long been in the focus of geological research. However, previous work has largely concentrated on sequence stratigraphy and sedimentary environment (Wang et al., 2005; Sun et al., 2011; Meng et al., 2016), fossil plants (Zhou and Sun, 1985; Manchester et al., 2005), lake paleoproductivity and organic matter accumulation (Meng et al., 2011, 2012; Sun et al., 2013; Xie et al., 2014; Zhang et al., 2014; Strobl et al., 2015; Volkman et al., 2015), and industrial utilizations (Bai et al., 2015; Jiang et al., 2015; Ren et al., 2015; Sun et al., 2015) of oil shale and coal. In contrast, only few studies reported on the provenance of the sedimentary material and paleoclimatic and environmental changes.

In this study mineralogical and geochemical methods are employed to oil shale and mudstones samples from the Huadian Formation to characterize the source rocks and to reconstruct Eocene paleoclimatic and environmental changes. In addition, the geochemical record of the Eocene Huadian Basin may also improve our understanding of the variability and environmental response of the East Asian monsoon climate (Quan et al., 2012).

## 2. Geological setting

The Eocene Huadian Basin is located in the central section of the Dunhua-Mishan Fault Zone in northeast China and belongs to a series of small fault-controlled basins (Fig.1a, b). The Huadian Basin covers an area of about 40 km<sup>2</sup> (Fig.1c). Towards the south, the basin is bordered by the F1 fault, a synsedimentary basin-controlling fault (Sun et al., 2013). The thickness of the basin fill increases southwards towards the F1 fault.

The basement of Huadian Basin includes granite and Permo-Carboniferous sedimentary rocks, which are overlain by Jurassic coal-bearing rocks and Cretaceous sandstones and conglomerates. The Huadian Basin itself is filled by the Eocene Huadian Formation, which is up to 1500 m thick and subdivided from bottom to top into three members: (1) the Pyrite Member, (2) the Oil Shale Member and (3) the Carbonaceous Shale Member.

The Pyrite Member represents the initial subsidence stage of the basin evolution. The lake ("Huadian lake") was in a state of

over-compensation deposition and filled with alluvial fans, fan delta and shallow lake sediments with limited areal extent (Sun et al., 2013). The lower part of the Pyrite Member is composed of gray mudstone intercalated with thin layers of sandstone containing pyrite layers (locally recoverable). The upper part comprises mainly brick red to purple and green mudstone, intercalated with thin gypsum layers.

The Oil Shale Member represents the maximum subsidence stage of the basin evolution. During deposition of the Oil Shale Member, the lake reached its largest extent and was filled with fine-grained sediments containing gray to dark gray mudstone and oil shale deposited in semi-deep and deep lake environment, intercalated with thin layers of gray-white fine-grained sandstone deposited in shallow lake and fan-delta front environment (Sun et al., 2013). The total number of oil shale layers varies from 6 to 26, but only 13 layers (numbered from top to bottom; Fig.2) are suitable for oil shale exploitation.

The Carbonaceous Shale Member represents the final basin-

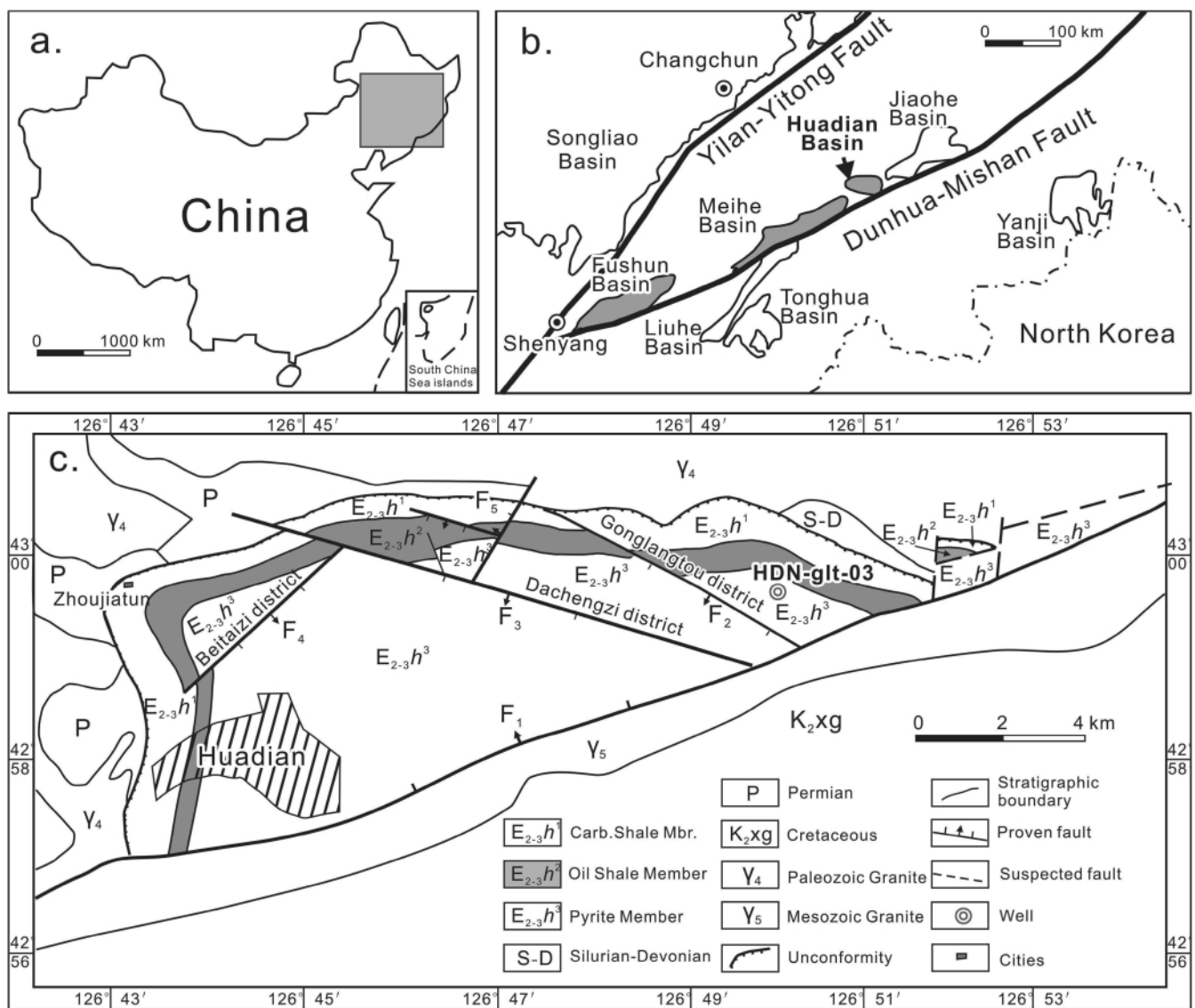
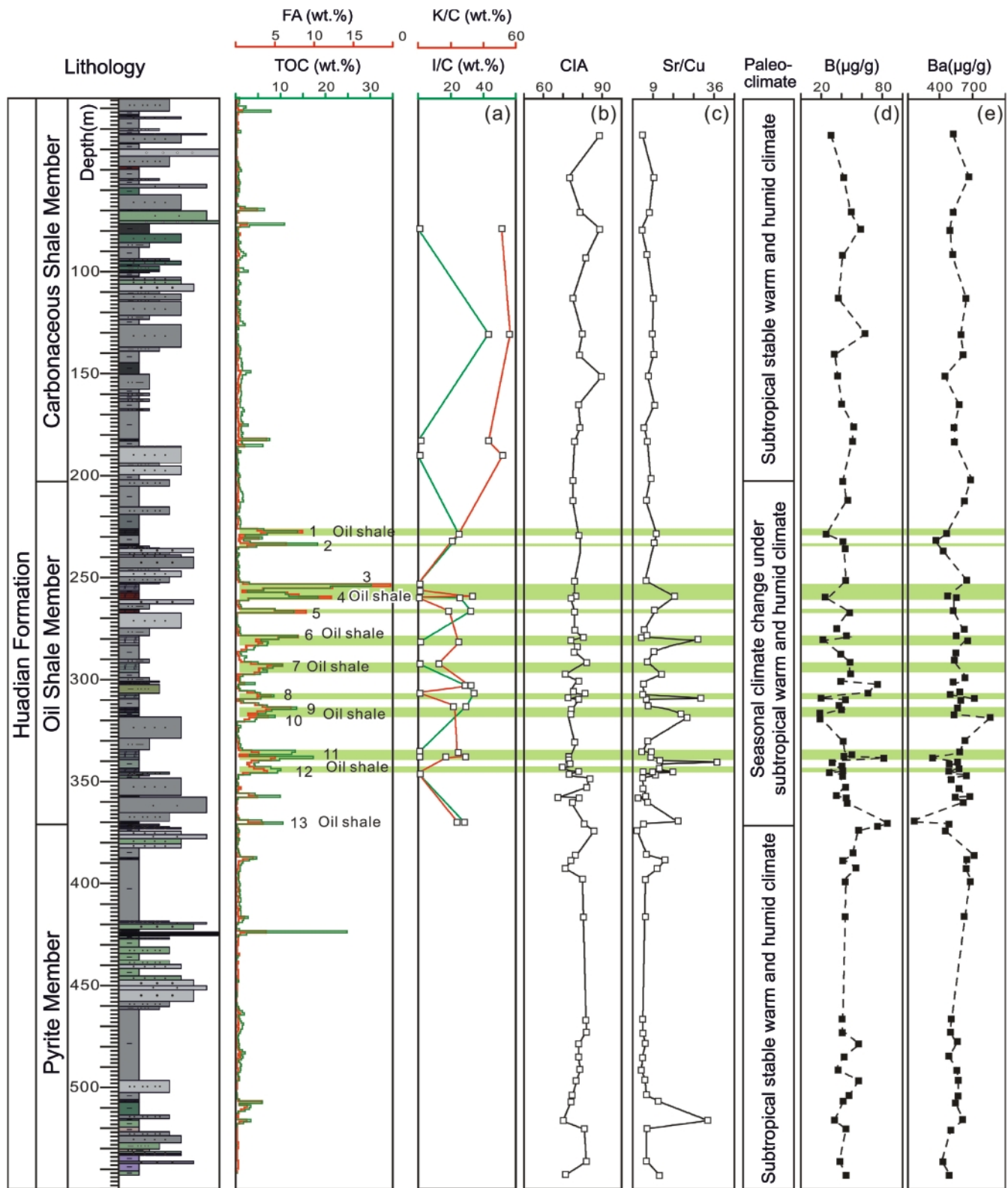


Figure 1: Geological map of the Huadian Formation (modified according to Sun et al., 2013).

filling stage when decreasing tectonic activity and increasing sediment supply caused filling of the basin (Sun et al., 2013). It includes fan delta and shallow, largely carbonate-free lake sediments (Strobl et al., 2015). The lower part contains gray mudstone interbedded with medium to coarse sandstone

and 18 thin coal layers. Four coal layers are mined locally. The middle part is represented by thick mudstone, whereas the upper part is composed of light gray mudstone interbedded with gray-white medium to fine sandstone. The Huadian Formation is covered by Quaternary sediments.

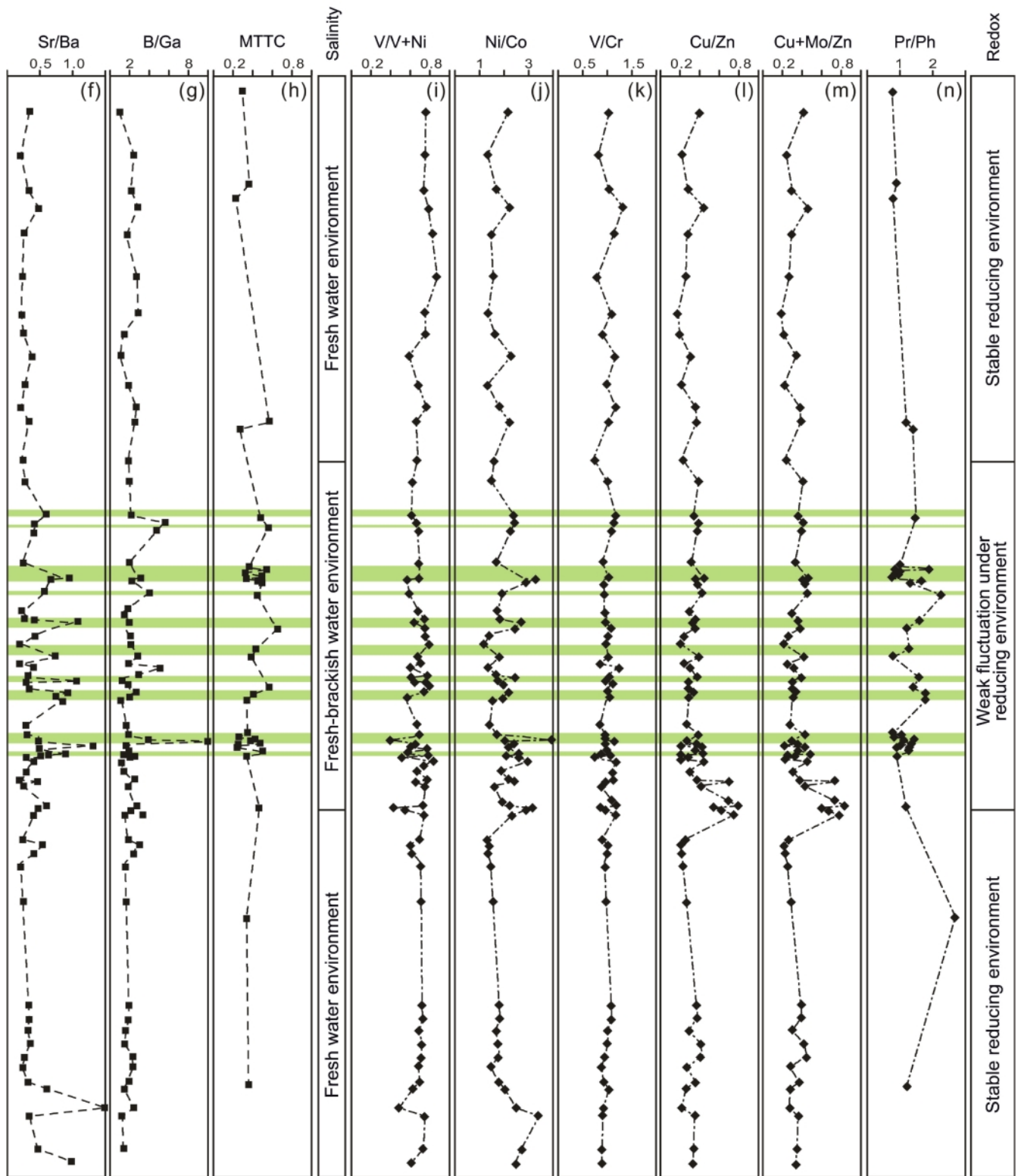


**Figure 2:** Vertical distributions of Fischer assay oil yield (FA), total organic carbon (TOC), the ratios of kaolinite versus clay minerals (K/C) and illite (MTTC) and n: Pristane/Phytane (Pr/Ph) after Strobl et al. (2015).

### 3. Materials and methods

A total of 78 fresh core samples including 18 oil shale (oil yield  $>3.5\%$ ) and 60 mudstone samples (oil yield  $<3.5\%$ ) were collected from the fully cored borehole HDN-glt-03, located in the northeastern part of the Huadian Basin (Gonglangtou

district, Fig.1c). The core is 542.8 m long and represents the entire Huadian Formation (98% core recovery). 16 samples were collected in the Pyrite Member (542.8–371.3 m), 49 samples in the Oil Shale Member (371.3–203.1 m), and 13 samples in the Carbonaceous Shale Member (203.1–16.9 m). Sample



versus clay minerals (I/C), CIA, typical trace elements and their ratios in the Huadian Formation. Biomarker data (h: Methyltrimethyltridecylchroman

selection was mainly based on data for Fischer assay oil yield (FA, wt.%) and total organic carbon (TOC, wt. %), which have been available for composite samples representing 1-m-thick intervals (see Sun et al., 2013 and Fig. 2).

X-ray diffraction analyses for 22 samples were performed at the Test Center of Jilin University (Changchun, China). The pulverized samples ( $\leq 200$  mesh) were investigated using a Philips PW1830 diffractometer system with Cu-K $\alpha$  radiation. Quantitative interpretation of minerals was carried out with a Siroquant™ XRD processing system (Taylor, 1991) using the dataset of Rietveld (1969).

Major, trace and rare earth elements (REEs) analysis for 78 samples have been determined at the Institute of Geophysical and Geochemical Exploration of the Chinese Academy of Geological Sciences (Langfang, China). Dried powdered samples were digested using lithium metaborate fusion. After heating to  $\sim 1200^{\circ}\text{C}$  glass plates were produced. The concentration of SiO<sub>2</sub> was determined by X-ray fluorescence (XRF) following the criteria of GB/T 14506.28-2010 (National Stand-

ards in China), whereas concentrations of Al<sub>2</sub>O<sub>3</sub>, Fe<sub>2</sub>O<sub>3</sub>, MgO, CaO, Na<sub>2</sub>O and K<sub>2</sub>O were determined using Inductively Coupled Plasma-Atomic Emission Spectrometry (ICP-AES) using Chinese National Standards (DZ/T 0223-2001). FeO was quantified using volumetric method (VOL). Trace element concentrations were determined by Emission Spectrometry (ES) (B), XRF (Zr), ICP-AES (Ba, Cr, Li, Mn, P, Rb, Sr, Ti, V) or Inductively Coupled Plasma Mass Spectrometry (ICP-MS) (Cd, Co, Cs, Cu, Ga, Hf, Mo, Nb, Ni, Pb, Sc, Th, Ta, U, Zn) following the criteria of National Standards in China (GB/T 14506.28-93 and DZ/T 0223-2001). The latter technique was also used to determine REE concentrations. The analytical precision for all elements was estimated to be <1-2% based on duplicate analysis.

To evaluate the paleoclimate and its influence on weathering, the chemical index of alteration (CIA; Nesbitt and Young, 1982) was calculated following the equation CIA=[Al<sub>2</sub>O<sub>3</sub>/ (Al<sub>2</sub>O<sub>3</sub>+CaO\*+Na<sub>2</sub>O+K<sub>2</sub>O)] $\times 100$ . In this equation all values are in molar proportions. CaO\* represents the amount of CaO incorporated into the silicate fraction of the rock. It is calculated

Basin	Sample numbers	Depth/m	FA Oil yield/wt.%	Relative content of mineral(%)											
				Terrigenous detrital minerals			Clay minerals			Carbonate minerals			Carbonate minerals		
				Quartz	Feldspar	Plagioclase	Smectite	Montmorillonite	Illite	Kaolinite	Calcite	Pyrite	Lepidocrocite	Gypsum	Siderite
<b>Carbonaceous Shale Member(E<sub>2-3</sub>h<sup>3</sup>)</b>															
Huadian	HD3-82	130.3	0.1	56	4	3		7	13	17					
	HD3-77	183	4	41		6	30			23					
	HD3-77B	185.5	0.3	25			36			39					
	<b>Oil Shale Member(E<sub>2-3</sub>h<sup>2</sup>)</b>														
	HD3-74	228.5	8.5	36		4	28		14	14	3	1			
	HD3-73	232	3	26	4		36		14	13		7			
	HD3-73B	251.7	0.2	35			38				27				
	HD3-72B	255	12.4	33	4		31				28	4			
	HD370B	258	6.6	42	2	2	34				17	3			
	HD3-71	259	8.1	32	3	3	25			11	19	2			5
	HD3-70	259.8	8.1	34			23		8		30	5			
	HD3-69	266.3	5	32	3		25		17	10	8	5			
	HD3-66B	281	2.6	42	2	3	24		8		19	2			
	HD3-63B	292.2	2	34	4	5	48			7		2			
	HD3-59B	305.5	0.5	23	2		18		14	15					28
	HD3-59	306.3	1.5	27			32		17		20				4
	HD3-55	312.7	2.5	50	4	6	19		12	9					
	HD3-49	336	3	39			44			14		3			
	HD3-48	337.6	0.5	38			22			9	16	3			12
	HD3-47	338.2	5.1	40	5	5	33		7		8	2			
	HD3-36	345.8	4.1	45	2	2	49					2			
	HD3-215	357.5	2.8	37	4	4	20		7	8	20				
	HD3-28	370.5	3.5		10		22		14	12		33	2		7

**Table 1:** Mineral abundances in the lake fine-grained clastic sediments from the Huadian Basin

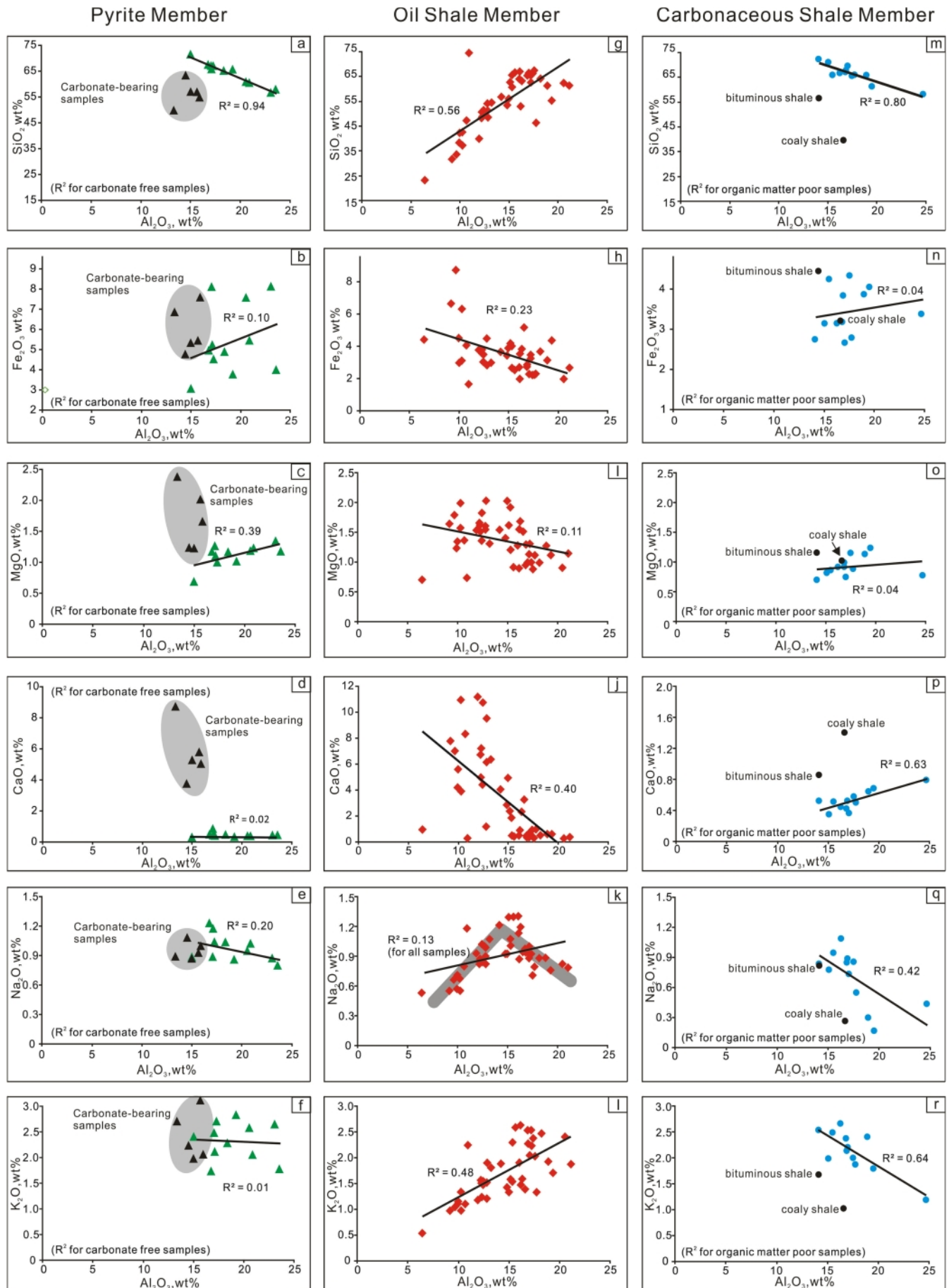


**Figure 3:** Major element oxide concentrations in fine-grained sediments in the Huadian Basin. (a, g, m) SiO<sub>2</sub> (b, h, n) Fe<sub>2</sub>O<sub>3</sub> (c, i, o) MgO (d, j, p) CaO (e, k, q)Na<sub>2</sub>O and (f, l, r)K<sub>2</sub>O plotted against Al<sub>2</sub>O<sub>3</sub> in order to analyze co-variation.

Sample numbers	Depth /m	Basin		TOC%	SiO <sub>2</sub> %	Al <sub>2</sub> O <sub>3</sub> %	Fe <sub>2</sub> O <sub>3</sub> %	FeO%	MgO%	CaO%	Na <sub>2</sub> O%	K <sub>2</sub> O%	SiO <sub>2</sub> /Al <sub>2</sub> O <sub>3</sub>	CIA	CIA <sub>(molar)</sub>
<i>Carbonaceous Shale Member</i>															
HD3-78	24	0.31	65.78	18.95	3.88	0.69	1.13	0.65	0.30	2.40	3.47	84	5.28		
HD3-77	32.7	0.22	61.30	19.50	4.05	0.55	1.23	0.69	0.17	1.80	3.14	89	7.76		
HD3-76	53.1	0.64	72.34	14.09	2.75	1.27	0.69	0.52	0.84	2.54	5.13	73	2.77		
HD3-75	70.2	2.17	65.77	17.50	4.36	1.55	1.15	0.58	0.86	2.00	3.76	79	3.77		
HD3-74	78.7	10.90	39.66	16.60	3.22	2.66	1.02	1.41	0.27	1.03	2.39	89	8.27		
HD3-73	92.39	1.86	65.98	17.72	2.79	1.09	0.88	0.50	0.55	1.87	3.72	82	4.62		
HD3-72	113	0.12	65.88	15.50	4.26	1.34	0.86	0.51	0.95	2.50	4.25	75	2.97		
HD3-71	130.3	0.23	69.67	17.02	2.67	1.34	0.74	0.37	0.74	2.22	4.09	80	3.96		
HD3-70	140.4	1.05	67.10	16.81	3.18	1.34	0.91	0.43	0.85	2.38	3.99	78	3.53		
HD3-69	150.9	3.43	58.18	24.68	3.39	1.52	0.77	0.80	0.44	1.19	2.36	90	9.01		
HD3-68	165	1.08	67.79	16.88	3.85	2.02	0.98	0.52	0.89	2.14	4.02	78	3.56		
HD3-67	176	2.82	70.99	15.07	3.15	1.34	0.81	0.35	0.78	1.99	4.71	79	3.69		
HD3-66	183	7.66	56.56	14.10	4.45	3.26	1.15	0.86	0.82	1.68	4.01	76	3.12		
HD3-65	200.7	0.93	66.86	16.24	3.15	1.66	0.91	0.45	1.09	2.67	4.12	75	2.95		
<i>Oil Shale Member</i>															
HD3-64	212	1.53	65.75	15.34	3.89	1.80	1.20	0.51	1.07	2.30	4.29	75	2.95		
HD3-63	228.5	13.90	37.30	10.26	9.27	7.12	1.57	3.91	0.55	0.98	3.64	78	3.57		
HD3-61	251.2	0.83	65.45	16.85	4.01	2.52	0.95	0.51	0.94	2.54	3.88	76	3.22		
HD3-60	259	11.90	31.63	9.19	9.80	8.73	1.64	7.77	0.55	0.98	3.44	76	3.20		
HD3-59	259.75		42.26	9.99	4.42	2.73	1.34	5.59	0.71	1.15	4.23	74	2.79		
HD3-58	266.26	8.90	38.13	9.92	6.63	3.99	1.23	4.22	0.57	1.11	3.84	76	3.22		
HD3-57	275.5	1.02	65.34	17.20	5.08	2.99	1.13	0.66	0.88	2.54	3.80	76	3.18		
HD3-56	279	13.80	61.21	18.88	4.60	2.31	1.27	0.63	0.88	1.93	3.24	80	4.02		
HD3-55	280.6	9.64	42.43	10.26	4.57	2.09	1.99	10.96	0.67	1.34	4.14	74	2.80		
HD3-54	283.31	7.10	56.04	14.98	5.70	2.81	2.03	4.96	0.92	1.33	3.74	77	3.35		
HD3-53	285.97	4.10	60.64	15.30	5.91	1.31	1.92	1.88	1.00	1.54	3.96	76	3.08		
HD3-52	291	2.02	67.48	17.56	3.26	1.34	0.88	0.32	0.71	2.04	3.84	82	4.43		
HD3-51	297.3	5.57	54.44	13.23	4.36	2.09	1.31	6.37	1.07	1.81	4.12	71	2.41		
HD3-50	300.54	0.98	64.08	18.21	5.41	2.77	0.99	0.55	0.88	2.47	3.52	78	3.55		
HD3-48	306.3	4.33	62.57	17.23	4.78	0.88	1.30	0.83	1.00	2.24	3.63	75	3.08		
HD3-47	307.2	5.47	55.36	19.36	6.40	2.27	1.11	0.61	0.76	1.71	2.86	82	4.59		
HD3-46	308.94	8.49	49.31	12.44	4.45	1.84	1.82	10.76	0.85	1.55	3.96	74	2.78		
HD3-45	309.6	5.60	65.60	16.88	4.20	0.88	1.29	0.38	0.98	2.28	3.89	78	3.53		
HD3-44	312.7	5.14	64.03	16.06	3.97	1.74	1.28	0.54	1.30	1.91	3.99	76	3.09		
HD3-43	314.4	13.60	51.26	12.81	4.16	1.95	1.60	6.16	0.90	1.52	4.00	74	2.78		
HD3-42	316.9	6.82	33.57	9.66	12.84	10.16	1.79	7.00	0.66	1.06	3.48	74	2.91		
HD3-41	318.6	8.94	39.94	11.93	5.57	1.74	1.54	11.18	0.93	1.19	3.35	73	2.74		
HD3-40	330.4	0.91	66.17	17.40	3.29	1.38	0.99	0.96	0.92	2.38	3.80	76	3.10		
HD3-39	335	13.30	66.48	17.04	3.36	1.31	0.99	0.41	0.94	2.05	3.90	79	3.78		
HD3-38	336	12.60	53.30	14.81	5.01	3.38	1.40	2.86	0.92	1.43	3.60	76	3.23		
HD3-36	338.2	17.30	23.11	6.43	6.47	2.66	0.70	0.94	0.53	0.55	3.59	73	2.75		
HD3-35	339.6	9.81	50.64	12.27	5.23	3.06	1.62	4.99	0.87	1.52	4.13	73	2.72		
HD3-34	340.2	5.15	48.55	12.85	5.64	2.63	2.03	9.56	0.82	1.90	3.78	73	2.70		
HD3-33	341.2	4.05	48.25	12.20	5.46	3.06	1.66	6.74	0.82	1.57	3.96	73	2.77		
HD3-32	342.2	4.44	63.18	16.31	5.65	1.84	1.68	2.35	1.19	1.59	3.87	74	2.89		
HD3-31	343.2	7.86	56.83	14.20	5.36	1.92	1.54	4.06	1.21	1.89	4.00	70	2.35		
HD3-30	344.5	10.10	47.23	10.68	5.96	2.99	1.36	8.35	0.80	1.11	4.42	74	2.78		
HD3-29	344.6		48.61	12.30	5.55	3.49	1.51	7.22	0.87	1.24	3.95	75	2.92		
HD3-27	344.8		51.39	12.43	5.12	2.95	1.36	4.43	1.02	1.48	4.13	71	2.50		
HD3-26	345.3	9.32	62.57	15.13	6.13	4.52	1.62	2.40	1.29	1.59	4.14	72	2.53		
HD3-25	345.8		54.12	12.80	6.59	1.31	1.54	1.20	0.99	1.21	4.23	74	2.80		

**Table 2:** Concentrations of typical major elements and respective ratios of the fine-grained clastic sediments in the Huadian Formation, Huadian

using the equation  $\text{CaO}^* = \text{CaO}-\text{CO}_2$  (calcite)-(0.5 \* $\text{CO}_2$  (dolomite)-(10/3× $\text{P}_2\text{O}_5$  (apatite) (Fedo et al., 2013). Dolomite is absent in the studied samples, but calcite is present in significant amounts in some samples. Because  $\text{CO}_2$  and  $\text{P}_2\text{O}_5$  data are absent, we followed an approach of McLennan et al. (1993) and Bock et al. (1998): If the mole fraction of  $\text{CaO} \leq \text{Na}_2\text{O}$ , then the value of  $\text{CaO}$  is accepted; if however,  $\text{CaO} > \text{Na}_2\text{O}$ , then we assumed that the moles of  $\text{CaO}^*=\text{Na}_2\text{O}$ . A similar index ( $\text{CIA}_{(\text{molar})}=\text{Al}_2\text{O}_{3(\text{molar})}/(\text{CaO}^*_{(\text{molar})}+\text{Na}_2\text{O}_{(\text{molar})}+\text{K}_2\text{O}_{(\text{molar})})$ ) was introduced by Goldberg and Humayun (2010).

## 4. Results

### 4.1 Mineralogy

The results of XRD analysis (n=22; Table 1) indicate that the fine-grained sediments include on average 35.3% quartz, 3.9% feldspar, 29.0% smectite, 5.9% illite, 9.8% kaolinite, and 9.8% calcite. Montmorillonite, pyrite, lepidocrocite, gypsum and siderite occur in minor amounts.

The mineral assemblages of sediments in the Oil Shale and Carbonaceous Shale members from the Huadian Basin differ significantly (Table 1). The average percentage of calcite in the Oil Shale Member is 11.3%. XRDs of three samples from the Carbonaceous Shale Member did not show carbonate minerals.

### 4.2 Major elements

Major element concentrations, expressed as weight per-

centages of oxides, are listed in Table 2. The sum of the major elements oxides varies significantly, mainly as a function of varying amounts of organic matter. Different major elements oxides are plotted against  $\text{Al}_2\text{O}_3$  in Fig. 3 to describe their covariance.

#### *Pyrite Member*

Samples from the Pyrite Member are characterized by high average contents of  $\text{SiO}_2$  (61.4%),  $\text{Al}_2\text{O}_3$  (17.7%) and  $\text{Fe}_2\text{O}_3$  (5.6%) and by low concentrations of  $\text{FeO}$ ,  $\text{MgO}$ ,  $\text{Na}_2\text{O}$ ,  $\text{K}_2\text{O}$  (Table 2).  $\text{CaO}$  contents are typically very low (<0.8%), but range from 3.7 to 8.7% in five carbonate-bearing samples. Whereas there is no good correlation between  $\text{Al}_2\text{O}_3$  and other major element oxides (Fig. 3b-f), there is a strong negative correlation between  $\text{Al}_2\text{O}_3$  and  $\text{SiO}_2$  ( $R^2=0.94$ ; Fig. 3a) for carbonate-free samples.

#### *Oil Shale Member*

The average contents of  $\text{SiO}_2$  (54.5%),  $\text{Al}_2\text{O}_3$  (14.4%),  $\text{Fe}_2\text{O}_3$  (5.2%) and  $\text{K}_2\text{O}$  (1.7%) in the Oil Shale Member are lower than in the Pyrite Member, a consequence of abundant organic matter. In contrast, the average  $\text{CaO}$  content (3.4%) is high reflecting increased calcite contents in oil shales.  $\text{FeO}$ ,  $\text{MgO}$ ,  $\text{Na}_2\text{O}$  occur in similar concentrations as in the Pyrite Member (Table 2). The observed moderate positive correlations between  $\text{Al}_2\text{O}_3$ ,  $\text{SiO}_2$  (correlation coefficient  $R^2=0.56$ ) and  $\text{K}_2\text{O}$  ( $R^2=0.48$ ; Fig. 3g,l).  $\text{Al}_2\text{O}_3$  and  $\text{Na}_2\text{O}$  correlate positively in samples with low  $\text{Al}_2\text{O}_3$  contents, but negatively in  $\text{Al}_2\text{O}_3$ -rich samples (Fig. 3k). Overall the correlation coefficient is low

Sample numbers	Depth /m	Basin											
		TOC%	$\text{SiO}_2\%$	$\text{Al}_2\text{O}_3\%$	$\text{Fe}_2\text{O}_3\%$	$\text{FeO}\%$	$\text{MgO}\%$	$\text{CaO}\%$	$\text{Na}_2\text{O}\%$	$\text{K}_2\text{O}\%$	$\text{SiO}_2/\text{Al}_2\text{O}_3$	CIA	$\text{CIA}_{(\text{molar})}$
HD3-24	346.8	3.23	66.81	15.62	3.69	0.77	0.91	0.43	1.29	2.59	4.28	73	2.74
HD3-23	348	0.76	61.31	21.12	3.92	0.70	1.14	0.40	0.78	1.88	2.90	84	5.22
HD3-22	352.6	0.36	62.26	20.55	2.91	1.09	0.90	0.30	0.82	2.41	3.03	82	4.55
HD3-21	357.1	9.91	74.41	10.92	2.42	0.00	0.72	0.31	1.18	2.25	6.81	69	2.21
HD3-20	357.7		52.89	16.18	5.19	3.74	1.55	0.90	0.87	1.48	3.27	78	3.62
HD3-19	359.8	0.18	67.03	16.13	2.87	0.56	0.90	0.30	1.13	2.63	4.16	75	3.07
HD3-17	370.5	10.70	46.23	17.76	3.38	2.45	1.11	0.99	0.79	1.33	2.60	81	4.39
<i>Pyrite Member</i>													
HD3-16	373.9	0.60	57.84	23.55	3.96	0.74	1.17	0.41	0.79	1.75	2.46	86	5.98
HD3-15	385.9	0.85	66.73	17.25	4.46	1.88	0.99	0.35	1.03	2.69	3.87	77	3.29
HD3-14	388.2	3.14	56.77	14.99	5.27	3.45	1.21	5.19	0.87	1.97	3.79	75	3.00
HD3-13	392.2	1.07	62.94	14.51	4.71	2.34	1.22	3.71	1.07	2.21	4.34	71	2.45
HD3-12	397.2	0.72	65.60	19.21	3.72	1.59	1.01	0.26	0.85	2.81	3.41	80	3.90
HD3-11	472.1	1.06	60.35	20.88	5.44	2.84	1.21	0.33	1.02	2.03	2.89	82	4.66
HD3-10	478.7	0.87	65.37	17.11	5.18	2.52	1.09	0.35	1.17	2.09	3.82	78	3.54
HD3-09	484.8	1.65	67.13	16.76	4.91	1.98	1.16	0.45	1.22	1.73	4.01	78	3.57
HD3-08	490.85	1.16	64.75	18.35	4.83	2.12	1.16	0.39	1.03	2.28	3.53	79	3.76
HD3-07	496.45	0.27	71.08	14.99	3.01	1.37	0.67	0.28	0.86	2.39	4.74	77	3.32
HD3-06	503.65	0.35	66.75	17.06	8.05	4.69	1.25	0.80	0.88	2.46	3.91	75	3.06
HD3-05	507	0.92	54.41	15.89	7.54	2.66	1.65	5.01	0.99	2.04	3.42	74	2.90
HD3-04	516.2	1.80	49.47	13.33	6.81	2.41	2.38	8.70	0.89	2.68	3.71	70	2.28
HD3-03	520.2	0.03	60.37	20.55	7.52	0.94	1.17	0.34	0.94	2.57	2.94	81	4.15
HD3-02	536.1	0.04	56.21	23.05	8.08	1.23	1.32	0.36	0.86	2.63	2.44	82	4.68

**Table 2:** continued

Sample number	Depth /m	Concentration ( $\mu\text{g/g}$ )																
		Co	Ni	V	Cr	Sr	Rb	Ba	Th	Sc	Nb	Ta	Zr	Hf	U	B	Cd	Cs
<i>Carbonaceous Shale Member</i>																		
HD3-78	24	13.5	32.1	98.4	80.9	176.8	116.7	578.9	15.6	12.7	35.8	2.4	264.2	6.0	3.2	27.4	50.6	8.9
HD3-77	32.7	15.8	34.3	108.1	103.2	177.2	93.3	519.3	14.9	12.7	31.4	2.2	246.7	6.1	4.3	29.8	82.9	7.9
HD3-76	53.1	15.1	20.2	62.8	75.7	142.5	109.2	664.2	14.6	9.7	38.8	2.7	322.5	7.2	3.6	42.0	338.0	6.3
HD3-75	70.2	17.1	29.1	81.6	78.6	167.4	109.5	520.7	16.5	13.6	23.9	1.9	191.9	5.1	3.4	48.9	257.2	9.4
HD3-74	78.7	12.5	28.2	102.1	77.0	233.0	78.0	488.3	17.5	14.6	15.5	1.2	144.7	3.7	4.2	57.9	367.8	7.0
HD3-73	92.4	11.8	17.4	81.8	72.3	130.6	95.2	515.9	14.1	11.3	26.3	2.1	221.2	5.8	3.6	41.1	355.2	9.2
HD3-72	113	6.9	10.9	76.9	96.5	151.0	84.9	641.0	10.5	8.1	8.8	0.8	309.6	7.9	1.3	37.4	86.5	8.4
HD3-71	130.3	16.8	22.7	70.1	64.9	127.0	103.8	588.3	12.8	10.1	28.5	2.2	228.4	5.9	3.2	63.7	192.0	7.8
HD3-70	140.4	16.0	26.2	80.8	89.3	155.2	114.9	615.6	13.0	10.9	33.2	2.3	209.4	5.2	3.0	33.7	161.4	8.0
HD3-69	150.9	31.8	73.6	105.5	89.4	166.0	67.8	443.0	19.4	14.0	25.5	2.0	166.9	4.4	3.7	36.4	136.6	7.4
HD3-68	165	25.2	33.7	72.3	73.2	156.6	103.9	573.2	14.0	11.3	27.0	2.0	177.8	4.5	3.2	40.7	220.8	8.2
HD3-67	176	12.9	23.4	77.3	65.7	116.3	107.7	532.8	18.3	10.9	30.2	2.5	235.4	6.1	4.8	52.4	369.1	8.1
HD3-66	183	18.9	42.0	82.0	79.5	177.2	95.5	534.0	15.3	10.0	18.9	1.4	160.0	4.2	3.2	50.5	183.7	6.9
HD3-65	200.7	23.1	37.4	78.9	108.4	155.2	120.9	685.1	15.6	10.7	34.0	2.4	302.9	7.5	3.6	42.1	203.1	7.2
<i>Oil shale Member</i>																		
HD3-64	212	37.1	55.7	92.3	92.5	174.8	115.4	623.0	16.1	10.9	31.1	2.2	251.1	6.3	3.9	45.0	241.2	7.7
HD3-63	228.5	18.4	44.5	70.4	59.6	265.4	71.0	455.0	10.9	9.3	9.5	0.7	113.0	2.6	2.1	25.3	178.1	5.5
HD3-62	232	9.1	22.2	44.9	38.9	159.5	37.3	354.7	5.7	5.8	6.5	0.5	88.6	2.3	1.3	42.0	112.5	3.4
HD3-61	251.2	21.9	37.2	86.4	94.6	155.3	125.7	646.6	16.9	11.5	35.1	2.4	272.2	6.5	3.8	44.6	217.8	7.5
HD3-60	259	8.3	23.3	52.2	50.1	401.9	62.5	464.9	8.4	7.9	8.1	0.6	82.9	1.9	1.6	28.5	139.4	4.6
HD3-59	259.8	11.6	36.7	50.1	53.8	346.5	83.9	527.9	8.8	7.4	10.3	0.8	93.1	2.3	1.9	24.9	105.1	5.4
HD3-58	266.3	20.3	39.6	56.3	59.0	297.0	84.5	522.9	9.9	8.5	12.2	0.9	120.8	2.3	2.3	47.0	369.6	5.2
HD3-57	275.5	23.6	41.1	93.6	99.6	146.8	133.0	612.2	17.0	12.4	37.6	2.7	253.6	5.7	3.9	34.0	208.5	8.0
HD3-56	279	19.9	37.1	108.5	106.1	183.2	121.6	532.1	17.2	15.5	27.7	2.0	217.8	5.1	3.9	47.5	149.6	9.2
HD3-55	280.6	11.3	29.6	53.3	54.7	642.8	82.5	631.6	9.1	8.5	10.3	0.8	90.4	2.3	1.5	24.0	248.3	5.5
HD3-54	283.3	9.8	24.3	75.9	70.0	407.6	91.6	584.1	11.4	10.7	15.6	1.2	139.1	3.5	2.5	29.5	149.2	7.6
HD3-53	286.0	19.2	28.5	83.8	83.2	259.2	109.5	547.9	15.2	11.6	15.5	1.2	126.2	3.7	1.8	36.1	244.3	8.1
HD3-52	291	17.7	21.1	78.9	80.3	119.0	112.1	526.6	15.9	12.3	29.4	2.3	246.5	6.5	3.6	47.9	283.5	9.4
HD3-51	297.3	17.3	31.7	66.4	64.4	456.7	108.9	621.1	13.5	10.6	19.0	1.5	173.7	4.6	2.6	48.6	469.4	7.0
HD3-50	300.5	25.5	39.1	92.4	108.2	145.1	136.1	627.4	17.4	16.0	34.8	2.5	249.7	6.0	3.8	40.5	236.8	8.2
HD3-49	302.1	41.6	55.7	83.4	67.4	206.3	92.1	505.4	11.5	9.4	18.4	1.1	208.8	3.7	2.5	74.7	887.5	5.5
HD3-48	306.3	17.8	30.6	102.8	102.0	190.5	124.2	593.8	17.3	13.7	30.8	2.3	205.9	5.5	3.2	66.4	266.4	8.4
HD3-47	307.2	25.5	61.2	97.1	93.1	169.7	116.6	479.5	18.9	12.6	25.8	1.9	200.4	5.2	3.5	40.7	182.2	8.4
HD3-46	308.9	19.7	34.7	65.4	67.3	741.4	122.8	680.6	12.0	10.2	14.1	1.1	106.4	2.7	1.6	19.6	271.5	7.0
HD3-45	309.6	18.5	35.0	111.7	101.4	180.7	138.6	591.6	20.0	14.8	38.6	2.9	246.9	5.6	4.7	43.0	254.8	9.6
HD3-44	312.7	11.7	24.1	86.2	84.2	198.3	118.7	577.6	17.1	12.4	22.1	1.7	224.5	5.4	3.4	39.1	291.5	8.8
HD3-43	314.4	11.2	24.6	67.3	65.6	503.1	112.3	558.5	12.3	10.5	15.5	1.2	111.5	3.1	1.7	42.6	335.7	7.1
HD3-42	316.9	21.8	42.4	55.2	51.4	392.5	70.0	520.3	9.3	8.3	11.9	1.0	87.3	2.3	1.7	19.1	157.1	5.2
HD3-41	318.6	33.8	52.4	67.8	69.4	703.8	107.0	859.4	12.6	17.1	12.6	1.0	114.6	2.8	4.2	19.4	565.5	6.8
HD3-40	330.4	30.2	43.3	89.1	103.6	179.0	129.3	611.1	17.2	12.5	36.3	2.5	282.0	6.7	3.8	41.9	199.0	8.4
HD3-39	335	25.2	43.6	97.5	100.2	178.6	126.0	586.5	19.9	14.3	37.9	2.7	295.8	6.8	4.3	43.1	306.9	8.7
HD3-38	336	15.6	44.4	78.2	78.6	276.0	103.2	567.8	13.2	12.3	18.3	2.5	155.8	4.0	2.4	46.7	293.6	7.9
HD3-37	337.6	20.5	79.7	49.6	52.6	178.5	72.0	367.8	10.1	7.7	10.3	0.8	104.3	2.9	1.7	48.4	286.6	5.9
HD3-36	338.2	27.6	53.6	56.4	47.2	164.0	37.7	336.0	6.2	7.2	6.8	0.5	64.1	1.8	1.4	86.6	167.2	3.8
HD3-35	339.6	14.9	34.5	66.9	69.6	423.4	113.1	479.4	11.1	8.8	13.5	1.0	122.2	3.1	1.4	37.2	534.4	7.0
HD3-34	340.2	17.8	38.4	67.4	68.9	727.8	129.4	565.8	11.5	10.5	14.7	1.2	105.7	3.0	1.5	30.9	300.3	8.0
HD3-33	341.2	17.8	39.2	61.1	63.9	493.4	122.2	528.6	10.5	9.4	14.2	1.1	107.0	2.9	1.5	31.5	378.9	7.4
HD3-32	342.2	8.6	19.9	88.2	88.1	264.5	107.1	491.8	13.3	13.0	22.2	1.7	177.0	4.6	2.0	43.0	76.6	9.0
HD3-31	343.2	20.0	48.1	77.3	76.2	378.3	114.8	568.1	13.0	12.2	17.8	1.4	171.1	4.5	2.8	34.3	437.5	7.3
HD3-30	344.5	16.1	42.4	53.8	60.9	481.0	89.9	505.0	11.4	8.6	12.7	1.0	47.9	1.2	1.8	27.2	351.2	6.0
HD3-29	344.6	13.7	33.0	58.6	64.5	432.6	105.6	535.0	11.4	10.2	13.3	1.1	87.1	2.4	1.7	32.7	291.3	6.9

**Table 3:** Trace elements concentration and respective ratios of the fine-grained clastic sediments in the Huadian Formation, Huadian Basin

Cu	Ga	Li	Mn	Mo	P	Pb	Ti	Zn	Sr/Ba	Sr/Cu	B/Ga	V/Cr	Ni/Co	V/(V+Ni)	Cu/Zn	(Cu+Mo)/Zn
19.4	27.0	45.1	138.6	1.0	152.7	26.2	7034.5	67.0	0.31	9.09	1.02	1.22	2.37	0.75	0.29	0.30
39.9	30.8	50.3	73.1	1.0	167.8	29.2	6063.1	99.4	0.34	4.44	0.97	1.05	2.17	0.76	0.40	0.41
15.4	17.1	29.3	232.0	1.0	196.6	22.9	8875.0	69.6	0.21	9.25	2.47	0.83	1.34	0.76	0.22	0.24
22.3	22.7	37.7	1588.6	1.3	248.1	25.1	6002.2	78.9	0.32	7.51	2.15	1.04	1.70	0.74	0.28	0.30
57.2	19.9	45.2	193.3	2.0	140.2	22.9	3311.3	128.9	0.48	4.07	2.90	1.33	2.26	0.78	0.44	0.46
19.5	24.4	42.3	216.5	1.1	152.4	25.6	6793.4	71.6	0.25	6.68	1.69	1.13	1.47	0.82	0.27	0.29
16.4	13.4	37.7	454.4	0.4	242.3	18.1	7488.2	63.0	0.24	9.21	2.79	0.80	1.58	0.88	0.26	0.27
14.4	21.9	41.8	161.0	1.0	145.0	22.8	6843.4	79.5	0.22	8.84	2.91	1.08	1.36	0.75	0.18	0.19
16.6	24.3	42.1	223.0	0.9	203.0	25.2	7352.9	84.9	0.25	9.33	1.39	0.90	1.64	0.76	0.20	0.21
24.6	35.0	74.5	262.3	2.6	1282.0	37.9	6669.2	79.3	0.37	6.75	1.04	1.18	2.32	0.59	0.31	0.34
16.2	21.8	39.2	1285.8	1.2	283.9	22.9	6718.1	78.3	0.27	9.66	1.87	0.99	1.34	0.68	0.21	0.22
22.5	19.3	32.5	497.8	1.1	289.1	32.1	8109.9	62.5	0.22	5.17	2.71	1.18	1.82	0.77	0.36	0.38
26.6	19.8	36.9	205.3	1.2	302.6	23.4	4509.8	71.1	0.33	6.65	2.55	1.03	2.22	0.66	0.37	0.39
19.5	22.2	41.6	337.0	0.9	231.3	25.6	7846.7	89.2	0.23	7.94	1.90	0.73	1.62	0.68	0.22	0.23
29.5	22.0	37.4	124.2	1.4	228.4	30.0	6987.0	75.8	0.28	5.92	2.05	1.00	1.50	0.62	0.39	0.41
24.7	11.8	19.8	2775.4	1.8	1036.0	17.1	2196.3	72.5	0.58	10.75	2.14	1.18	2.42	0.61	0.34	0.36
16.3	7.6	14.1	201.8	1.0	292.2	7.8	1378.7	42.3	0.45	9.78	5.53	1.15	2.44	0.67	0.39	0.41
27.6	22.2	44.2	483.5	1.0	314.0	25.9	7803.7	87.3	0.24	5.62	2.02	0.91	1.70	0.70	0.32	0.33
21.6	10.0	22.2	4364.9	1.0	930.8	13.0	2553.4	48.8	0.86	18.59	2.86	1.04	2.82	0.69	0.44	0.46
19.3	11.6	22.3	559.6	2.4	452.9	13.0	2516.2	52.3	0.66	17.93	2.16	0.93	3.17	0.58	0.37	0.42
29.8	11.8	25.1	1321.0	1.7	821.4	13.8	2713.4	69.1	0.57	9.96	3.97	0.95	1.95	0.59	0.43	0.46
28.2	25.6	47.7	779.6	1.0	720.0	27.2	7779.7	98.8	0.24	5.20	1.33	0.94	1.74	0.70	0.29	0.30
31.0	26.1	49.7	351.7	1.3	180.0	25.6	6237.1	86.9	0.34	5.91	1.82	1.02	1.86	0.75	0.36	0.37
23.6	12.0	24.0	1629.7	1.0	1400.0	14.4	2651.7	70.4	1.02	27.27	1.99	0.98	2.61	0.64	0.33	0.35
24.3	18.6	33.4	967.9	1.5	537.0	19.2	4064.7	67.0	0.70	16.74	1.58	1.09	2.49	0.76	0.36	0.39
27.3	19.4	24.1	857.7	1.2	681.8	18.7	4043.7	103.3	0.47	9.50	1.86	1.01	1.48	0.75	0.26	0.28
18.2	22.2	47.1	296.6	1.1	255.7	25.7	7955.0	88.8	0.23	6.53	2.15	0.98	1.19	0.79	0.21	0.22
35.6	16.7	28.7	1015.3	2.0	1361.0	21.5	4623.6	89.3	0.74	12.82	2.91	1.03	1.83	0.68	0.40	0.42
24.8	24.5	48.1	1638.6	1.1	375.4	25.7	8227.6	99.4	0.23	5.85	1.66	0.85	1.53	0.70	0.25	0.26
44.8	13.7	22.3	418.0	2.5	1569.0	14.5	3665.9	150.7	0.41	4.60	5.43	1.24	1.34	0.60	0.30	0.31
37.8	25.3	48.0	424.0	1.1	397.4	27.7	7134.4	105.6	0.32	5.04	2.63	1.01	1.72	0.77	0.36	0.37
34.5	28.7	61.1	410.1	1.8	544.9	43.0	5064.1	90.3	0.35	4.92	1.42	1.04	2.40	0.61	0.38	0.40
24.5	15.4	24.2	1326.9	1.0	2771.0	17.7	3467.6	88.8	1.09	30.29	1.27	0.97	1.76	0.65	0.28	0.29
28.8	24.7	45.5	265.9	1.4	241.5	31.6	9252.5	100.9	0.31	6.27	1.74	1.10	1.89	0.76	0.29	0.30
28.6	19.1	34.5	106.3	1.2	101.7	22.6	5970.8	99.5	0.34	6.94	2.05	1.02	2.06	0.78	0.29	0.30
31.7	16.6	25.5	658.9	1.0	1332.0	18.3	3720.8	95.2	0.90	15.87	2.56	1.03	2.20	0.73	0.33	0.34
17.6	12.3	22.1	9494.2	1.2	1493.0	13.9	2843.1	61.0	0.75	22.25	1.55	1.07	1.95	0.57	0.29	0.31
29.3	15.8	24.2	1371.0	1.0	22420.0	16.7	2742.7	101.5	0.82	24.02	1.23	0.98	1.55	0.56	0.29	0.30
27.4	24.7	45.2	229.9	1.0	1645.0	26.0	8136.0	100.6	0.29	6.52	1.70	0.86	1.43	0.67	0.27	0.28
38.0	22.5	41.5	153.3	1.8	232.7	27.8	8681.2	95.2	0.30	4.71	1.91	0.97	1.73	0.69	0.40	0.42
33.7	18.4	31.9	441.0	1.6	1742.0	20.3	4536.5	95.4	0.49	8.18	2.54	1.00	2.86	0.64	0.35	0.37
22.5	11.4	19.7	238.1	1.6	712.7	14.8	2555.8	75.1	0.49	7.93	4.23	0.94	3.89	0.38	0.30	0.32
15.6	7.8	14.0	118.9	2.3	24.9	8.3	1400.9	61.8	0.49	10.53	11.07	1.20	1.94	0.51	0.25	0.29
32.8	15.2	22.1	740.9	1.0	878.6	14.0	3332.5	94.3	0.88	12.93	2.44	0.96	2.31	0.66	0.35	0.36
17.8	16.9	23.3	1881.6	0.8	1474.0	17.8	3573.7	97.3	1.29	40.83	1.84	0.98	2.15	0.64	0.18	0.19
37.2	16.1	21.9	1323.0	1.2	3099.0	13.9	3347.7	86.9	0.93	13.26	1.95	0.96	2.20	0.61	0.43	0.44
21.5	22.5	30.7	647.3	1.0	133.2	19.2	5616.5	64.5	0.54	12.29	1.91	1.00	2.33	0.82	0.33	0.35
33.8	17.9	27.8	570.7	1.6	2227.0	20.6	4700.7	85.4	0.67	11.19	1.92	1.01	2.41	0.62	0.40	0.41
32.4	13.3	21.3	1714.0	1.4	1149.0	16.5	3051.8	71.7	0.95	14.83	2.05	0.88	2.63	0.56	0.45	0.47
30.7	14.8	23.9	1664.0	1.2	1215.0	15.7	3295.0	75.7	0.81	14.11	2.20	0.91	2.41	0.64	0.41	0.42

( $R^2 = 0.13$ ). A moderate negative correlation between  $\text{Al}_2\text{O}_3$  and  $\text{CaO}$  ( $R^2 = 0.40$ ; Fig. 3j) is due to the dilution of clay minerals by organic matter in carbonate-bearing oil shales. Although  $\text{Al}_2\text{O}_3$  and  $\text{K}_2\text{O}$  contents are positively correlated ( $R^2 = 0.48$ ; Fig. 3l), there is only a very weak negative correlation between  $\text{Al}_2\text{O}_3$  and  $\text{MgO}$  ( $R^2 = 0.11$ ; Fig. 3i).

#### *Carbonaceous Shale Member*

Samples from the Carbonaceous Shale Member show relative high average  $\text{SiO}_2$  (63.9%),  $\text{Al}_2\text{O}_3$  (17.2%) and  $\text{K}_2\text{O}$  (2.0%) contents, whereas average concentrations of  $\text{Fe}_2\text{O}_3$ ,  $\text{FeO}$ ,  $\text{MgO}$ ,  $\text{CaO}$  and  $\text{Na}_2\text{O}$  are lower than in any other member. If two organic matter-rich samples are excluded, a strong negative correlations exist between  $\text{Al}_2\text{O}_3$  and  $\text{SiO}_2$  ( $R^2 = 0.80$ ; Fig. 3m). Moderate negative correlations are also observed for  $\text{Al}_2\text{O}_3$ ,  $\text{Na}_2\text{O}$  ( $R^2 = 0.42$ ) and  $\text{K}_2\text{O}$  (0.64; Fig. 3q,r).  $\text{CaO}$  shows a strong positive correlation with  $\text{Al}_2\text{O}_3$  ( $R^2 = 0.80$ ; Fig. 3p) and displays a strongly negative correlation with  $\text{SiO}_2$  ( $R^2 = 0.93$ ).

Average major element oxide concentrations for each member of the Huadian Basin are normalized to the value for the upper continental crust (UCC; Taylor and McLennan, 1985) in

Fig. 4a. Ratios for  $\text{SiO}_2$ ,  $\text{Al}_2\text{O}_3$  and  $\text{Fe}_2\text{O}_3$  are close to 1, whereas  $\text{FeO}$ ,  $\text{MgO}$ ,  $\text{CaO}$ ,  $\text{Na}_2\text{O}$  and  $\text{K}_2\text{O}$  are depleted.

#### 4.3 Trace elements

Concentrations of 26 trace elements are listed in Table 3. Their average concentrations in the three members, normalized to the UCC, are shown in Fig. 4b. The distribution of the trace elements in the different members is similar.  $\text{Co}$ ,  $\text{Ni}$ ,  $\text{V}$ ,  $\text{Cr}$  as well as  $\text{B}$ ,  $\text{Cd}$ ,  $\text{Cs}$ ,  $\text{Li}$  and  $\text{Ti}$  are enriched relative to UCC. Most other trace elements occur in similar concentrations. In contrast,  $\text{Sr}$  concentrations are depleted, where  $\text{P}$  is strongly decreased in the Carbonaceous Shale Member.

#### 4.4 Rare-earth elements

Concentrations of 14 rare earth elements (REEs) and the sums of all REEs ( $\Sigma\text{REE}$ ), light REEs ( $\Sigma\text{LREE}$ ;  $\text{La}$ ,  $\text{Ce}$ ,  $\text{Pr}$ ,  $\text{Nd}$ ,  $\text{Sm}$ ,  $\text{Eu}$ ) and heavy REEs ( $\Sigma\text{HREE}$ ;  $\text{Gd}$ ,  $\text{Tb}$ ,  $\text{Dy}$ ,  $\text{Ho}$ ,  $\text{Er}$ ,  $\text{Tm}$ ,  $\text{Yb}$ ,  $\text{Lu}$ ) are presented in Table 4 together with some useful REE ratios.

The average  $\Sigma\text{REE}$  in the Pyrite, Oil Shale and Carbonaceous Shale members are 262  $\mu\text{g/g}$ , 194.4  $\mu\text{g/g}$ , 218  $\mu\text{g/g}$ , respecti-

Sample number	Depth /m	Concentration ( $\mu\text{g/g}$ )																	
		Co	Ni	V	Cr	Sr	Rb	Ba	Th	Sc	Nb	Ta	Zr	Hf	U	B	Cd	Cs	
HD3-28	344.7	19.1	49.1	85.6	86.1	294.0	110.2	490.6	13.8	14.2	18.6	1.4	/	/	2.7	31.8	156.0	8.7	
HD3-27	344.8	17.8	44.0	65.0	71.5	348.4	108.1	481.3	13.1	11.2	15.3	1.2	138.2	3.6	2.8	42.6	337.8	6.8	
HD3-26	345.3	9.6	20.3	84.5	87.1	277.6	111.4	530.9	13.7	13.4	18.7	1.4	151.5	4.3	1.9	32.0	139.7	8.2	
HD3-25	345.8	25.8	61.9	71.3	95.4	248.4	112.7	500.7	17.7	12.4	9.6	0.8	104.4	3.5	2.5	36.7	374.9	8.2	
HD3-24	346.8	14.4	40.7	84.4	99.8	175.4	121.4	673.8	15.0	12.1	28.7	2.0	332.4	8.3	3.8	39.7	40.6	6.7	
HD3-23	348	11.1	32.6	140.4	119.0	190.5	90.4	486.2	16.9	18.0	31.5	2.3	244.1	5.9	4.2	39.0	86.3	10.0	
HD3-22	352.6	32.4	60.9	121.3	108.9	164.2	114.8	560.9	19.3	12.8	29.1	2.1	351.8	8.2	3.8	43.1	109.1	9.3	
HD3-21	357.1	8.9	19.8	74.2	64.9	150.3	98.9	645.1	16.2	9.3	42.3	3.1	307.0	7.2	3.7	34.2	161.9	5.4	
HD3-20	357.7	20.2	48.5	85.5	89.6	228.8	119.3	531.2	18.6	15.1	14.2	1.1	128.8	3.4	3.6	44.9	363.0	9.4	
HD3-19	359.8	18.6	29.9	93.6	107.6	150.6	114.6	625.5	15.4	9.4	32.6	2.3	361.0	8.8	3.7	43.5	113.3	7.3	
HD3-18	369.5	3.4	6.8	18.5	15.6	74.5	12.1	120.8	1.5	3.8	3.6	0.1	57.7	1.4	0.6	86.6	37.0	1.1	
HD3-17	370.5	26.5	84.5	70.5	81.7	225.1	70.7	482.3	16.3	10.9	12.9	1.1	137.8	3.6	2.6	56.5	347.1	6.7	
<i>Pyrite Member</i>																			
HD3-16	373.9	22.5	52.7	153.9	129.6	185.9	116.3	445.5	18.0	20.7	26.2	1.9	226.7	5.5	5.7	50.7	79.6	11.0	
HD3-15	385.9	31.7	42.0	96.5	107.1	165.7	141.1	708.2	18.4	14.0	47.1	3.2	309.4	6.7	4.1	42.7	227.1	8.6	
HD3-14	388.2	41.2	58.6	88.8	88.1	352.7	121.7	644.8	15.8	13.0	27.2	1.9	207.5	4.8	3.2	54.8	383.7	7.3	
HD3-13	392.2	37.9	50.8	83.7	83.0	285.2	127.8	630.7	16.7	12.7	27.5	2.1	225.7	5.4	3.6	44.6	432.7	7.6	
HD3-12	397.2	26.5	38.7	93.2	98.3	140.4	146.9	675.7	17.5	15.3	42.2	3.0	265.6	6.2	4.6	41.1	251.1	8.9	
HD3-11	472.1	25.7	47.5	125.7	113.9	167.4	138.3	491.7	20.5	18.1	28.4	2.0	197.9	4.8	4.7	57.9	221.7	10.1	
HD3-10	478.7	27.8	46.4	105.8	103.7	176.1	133.4	548.1	19.0	16.1	36.0	2.5	248.7	5.5	4.2	42.8	255.8	8.7	
HD3-09	484.8	21.0	37.2	95.5	93.4	170.3	96.6	481.4	17.5	14.2	23.7	1.8	191.2	4.7	3.7	34.7	312.0	7.4	
HD3-08	490.9	23.5	42.7	110.0	114.1	154.2	130.8	552.6	18.5	17.0	31.4	2.2	236.1	5.6	3.9	57.1	278.8	8.4	
HD3-07	496.5	27.4	40.1	88.4	99.4	133.2	116.2	566.8	17.6	12.7	37.1	2.5	313.4	7.4	4.1	48.0	309.0	5.9	
HD3-06	503.7	23.2	41.6	95.7	103.4	177.7	136.7	564.7	18.7	15.7	39.9	2.7	220.7	5.1	3.6	41.7	215.1	7.4	
HD3-05	507	28.0	57.2	96.5	92.4	337.5	136.7	538.9	15.0	15.1	21.3	1.6	157.3	4.0	2.7	33.1	352.0	8.3	
HD3-04	516.2	29.9	74.7	71.4	77.1	928.8	149.1	614.7	12.2	11.7	15.9	1.2	74.2	2.0	1.8	44.5	334.7	6.8	
HD3-03	520.2	10.4	35.7	107.7	116.7	172.0	155.4	499.8	16.5	19.3	31.1	2.1	193.1	4.7	2.0	38.1	29.1	9.8	
HD3-02	536.1	16.2	44.0	123.2	137.3	193.8	150.5	414.0	18.9	22.6	28.9	2.0	222.9	5.5	2.2	44.7	91.0	11.6	
HD3-01	542.8	21.4	53.1	83.5	92.6	507.5	151.9	489.9	15.3	14.3	20.4	1.5	154.3	3.9	4.0	40.2	681.8	7.7	
UCC		10.0	20.0	60.0	35.0	350.0	112.0	550.0	10.7	11.0	25.0	2.2	190.0	5.8	2.8	15.0	98.0	3.7	

**Table 3:** continued

vely. The LREE/HREE ratios range from 7.8 to 13.4, reflecting a strong enrichment of LREEs in all fine-grained rocks. Fig. 4c shows that all elements are enriched in comparison to average UCC in all members. Chondrite-normalized REE abundances show a distinctly sloping LREE trend and a relatively flat HREE trend, with slightly negative Eu anomalies (Fig. 5a). High  $(\text{La/Yb})\text{N}$  (8.2–17.2) and  $(\text{Ce/Yb})\text{N}$  (5.1–29.4) ratios emphasize the obvious fractionation between LREEs and HREEs. Uniform REE patterns imply similar REE concentrations of source lithologies and/or no strong weathering effect on REE distribution (McLennan, 1989; Jin et al., 2006). The chondrite-normalized REEs of UCC and PAAS (Post-Archaean Australia Shale; Taylor and McLennan, 1985) are plotted together with the average chondrite-normalized REE concentrations of the fine-grained sediments in the Huadian Basin (Fig. 5b), showing similar patterns and abundances, especially to PAAS.

REEs may occur in fine-grained minerals and in organic matter. In the Pyrite Member, there is no correlation between  $\Sigma\text{REE}$  and TOC contents (Fig. 6a), but very weak positive ( $\text{SiO}_2$ ,  $\text{Al}_2\text{O}_3$ ) and negative ( $\text{Na}_2\text{O}$ ,  $\text{K}_2\text{O}$ ) correlations with major ele-

ment oxides (Fig. 6b–e). In the Oil Shale Member,  $\Sigma\text{REE}$  has a negative correlation with TOC (Fig. 6f), but positive correlation with  $\text{SiO}_2$ ,  $\text{Al}_2\text{O}_3$ ,  $\text{Na}_2\text{O}$  and  $\text{K}_2\text{O}$  (Fig. 6g–j). Maximum REE concentrations in the Carbonaceous Shale Member are observed in a coaly shale samples (Fig. 6k).

## 5. Discussion

The composition of sedimentary rocks is largely controlled by the lithologies of the source region and the intensity of weathering during erosion, transportation and deposition. This in turn can be altered by the downstream sorting during sediment transport and early post-depositional processes (McLennan, 1989, 2001; Johnsson, 1993; Weltje and Von Eynatten, 2004). Obviously, weathering is strongly influenced by paleoclimate. Hence, geochemical data may allow inferences about source rock composition, weathering and paleoclimate. Vitrinite reflectance (0.40–0.45 % Ro) and Tmax values (430–440 °C) indicate that the Huadian Formation is thermally immature (Strobl et al., 2015). Therefore, the mineralogical and geochemical data should not be strongly influenced by diagenetic processes.

Cu	Ga	Li	Mn	Mo	P	Pb	Ti	Zn	Sr/Ba	Sr/Cu	B/Ga	V/Cr	Ni/Co	V/(V+Ni)	Cu/Zn	(Cu+Mo)/Zn
27.0	21.7	33.0	569.2	1.7	309.3	32.2	4511.1	96.5	0.60	10.88	1.47	0.99	2.57	0.64	0.28	0.30
28.0	15.9	23.6	411.9	1.1	426.9	16.6	3672.9	73.4	0.72	12.43	2.69	0.91	2.47	0.60	0.38	0.40
14.3	20.4	26.8	843.0	0.9	1140.0	15.8	4803.5	70.1	0.52	19.45	1.57	0.97	2.12	0.81	0.20	0.22
47.5	15.1	19.9	222.0	1.2	153.8	14.2	2414.8	153.1	0.50	5.23	2.43	0.75	2.40	0.54	0.31	0.32
16.4	21.7	37.0	165.1	1.2	172.1	23.6	6586.6	85.3	0.26	10.67	1.82	0.85	2.82	0.67	0.19	0.21
43.2	32.9	63.6	70.4	1.7	200.8	28.8	6889.2	96.8	0.39	4.41	1.19	1.18	2.95	0.81	0.45	0.46
33.7	31.2	65.8	84.8	1.8	183.3	32.5	6363.6	117.6	0.29	4.87	1.38	1.11	1.88	0.67	0.29	0.30
25.1	14.6	27.3	136.9	1.3	182.8	28.1	10951.2	68.4	0.23	5.98	2.35	1.14	2.22	0.79	0.37	0.39
68.7	19.9	30.5	193.4	2.7	66.0	20.9	3525.2	94.9	0.43	3.33	2.26	0.95	2.41	0.64	0.72	0.75
23.6	23.9	44.5	102.3	1.0	176.7	23.6	7904.7	58.2	0.24	6.37	1.82	0.87	1.60	0.76	0.41	0.42
3.7	2.5	4.9	29.8	0.3	23.4	2.7	371.9	4.8	0.62	19.90	35.22	1.19	2.00	0.73	0.79	0.84
43.0	22.0	33.6	131.4	1.8	1083.0	13.1	3437.8	76.1	0.47	5.24	2.57	0.86	3.19	0.45	0.56	0.59
93.2	33.1	77.8	66.0	2.4	119.1	32.6	6115.8	124.8	0.42	1.99	1.53	1.19	2.34	0.74	0.75	0.77
25.6	23.4	41.8	576.0	1.2	296.2	27.5	10649.0	100.7	0.23	6.46	1.82	0.90	1.32	0.70	0.25	0.27
24.5	19.0	34.0	1238.7	1.4	1871.0	28.0	6211.4	119.0	0.55	14.37	2.89	1.01	1.42	0.60	0.21	0.22
24.6	18.3	32.9	804.5	1.4	1281.0	27.1	6763.5	116.5	0.45	11.62	2.43	1.01	1.34	0.62	0.21	0.22
24.6	26.1	53.8	352.1	1.2	274.7	28.6	10142.5	105.3	0.21	5.70	1.58	0.95	1.46	0.71	0.23	0.25
37.0	29.5	64.3	186.7	1.6	187.8	35.5	6869.2	97.3	0.34	4.52	1.96	1.10	1.85	0.73	0.38	0.40
30.9	25.3	45.0	133.8	1.3	344.7	30.6	8352.0	105.7	0.32	5.69	1.69	1.02	1.67	0.70	0.29	0.30
37.9	23.3	42.4	166.6	1.1	247.8	26.1	6086.2	92.1	0.35	4.50	1.49	1.02	1.77	0.72	0.41	0.42
39.1	25.1	44.6	238.1	1.4	161.3	26.6	7992.8	90.4	0.28	3.94	2.28	0.96	1.82	0.72	0.43	0.45
23.8	20.1	42.7	262.2	1.1	327.4	26.1	9790.7	89.0	0.23	5.61	2.38	0.89	1.47	0.69	0.27	0.28
29.2	23.4	51.0	2150.1	1.0	935.1	27.6	9288.8	80.8	0.31	6.09	1.79	0.93	1.80	0.70	0.36	0.37
28.1	22.6	42.1	2366.7	1.4	4203.0	22.4	4931.0	106.2	0.63	12.03	1.46	1.04	2.04	0.63	0.26	0.28
27.7	17.9	35.8	1379.8	5.2	1881.0	18.6	3626.4	123.9	1.51	33.54	2.49	0.93	2.50	0.49	0.22	0.27
27.3	29.4	61.6	119.0	1.0	101.0	25.7	7393.6	79.0	0.34	6.30	1.30	0.92	3.45	0.75	0.35	0.36
30.9	32.7	70.9	143.4	1.2	167.7	26.4	6782.7	91.7	0.47	6.28	1.37	0.90	2.71	0.74	0.34	0.35
42.9	21.9	31.8	753.1	0.9	4220.0	21.4	4836.2	129.7	1.04	11.83	1.84	0.90	2.48	0.61	0.33	0.34
25.0	17.0	20.0	600.0	1.5	700.0	20.0	3000.0	71.0	0.64	14.00	0.88	1.71	2.00	0.75	0.35	0.37

Sample numbers	Depth /m	La	Ce	Pr	Nd	Sm	Eu	Gd	Tb	Dy	Ho	Er	Tm	Yb	Lu	$\Sigma$ REE	$\Sigma$ LREE	$\Sigma$ HREE
<i>Carbonaceous Shale (with coal) Member</i>																		
HD3-78	24.0	47.88	84	8.80	30	5.15	1.01	4.0	0.66	3.73	0.75	2.10	0.40	2.20	0.37	191.5	177.3	14.2
HD3-77	32.7	58.59	117	11.82	42	7.72	1.54	5.6	0.97	4.98	0.92	2.37	0.43	2.42	0.38	256.6	238.6	18.1
HD3-76	53.1	53.24	111	10.53	37	6.71	1.38	5.2	0.90	4.92	0.99	2.70	0.52	2.87	0.48	238.7	220.2	18.6
HD3-75	70.2	49.80	97	10.08	36	6.45	1.35	5.3	0.91	5.02	1.03	2.85	0.53	2.97	0.50	219.5	200.4	19.1
HD3-74	78.7	97.87	167	19.97	76	13.71	2.74	10.6	1.71	8.81	1.65	4.23	0.76	3.96	0.65	409.8	377.5	32.3
HD3-73	92.4	43.77	87	8.81	31	5.58	1.07	4.4	0.78	4.37	0.88	2.50	0.47	2.64	0.43	193.7	177.3	16.5
HD3-72	113	42.55	82	8.53	30	5.18	1.06	4.0	0.67	3.67	0.74	2.09	0.40	2.22	0.36	184.0	169.8	14.2
HD3-71	130.3	39.69	70	7.69	27	4.76	0.90	3.8	0.66	3.75	0.76	2.09	0.41	2.29	0.37	164.3	150.2	14.1
HD3-70	140.4	43.00	79	8.54	30	5.07	1.02	3.9	0.66	3.62	0.73	2.07	0.40	2.24	0.36	180.7	166.7	14.0
HD3-69	150.9	44.22	70	8.42	30	5.27	1.11	4.2	0.71	3.84	0.76	2.08	0.38	2.12	0.35	173.0	158.5	14.5
HD3-68	165.0	41.27	79	8.11	28	4.89	0.96	3.9	0.65	3.70	0.74	2.10	0.40	2.27	0.39	176.2	162.0	14.1
HD3-67	176.0	54.73	106	11.36	42	8.10	1.60	6.6	1.18	6.63	1.32	3.75	0.70	3.83	0.61	249.0	224.4	24.6
HD3-66	183.0	45.50	84	9.32	34	6.20	1.25	4.9	0.82	4.50	0.89	2.39	0.46	2.47	0.41	196.3	179.5	16.8
<i>Oil Shale Member</i>																		
HD3-65	200.7	54.39	109	11.38	40	7.05	1.40	5.4	0.89	4.83	0.95	2.62	0.49	2.70	0.45	241.5	223.2	18.4
HD3-64	212.0	68.42	131	13.57	50	8.86	1.79	6.9	1.20	6.32	1.25	3.40	0.63	3.41	0.55	296.6	272.9	23.7
HD3-63	228.5	33.83	66	7.39	27	5.31	1.16	4.6	0.80	4.47	0.95	2.67	0.49	2.77	0.47	158.2	141.0	17.2
HD3-62	232.0	32.63	64	7.22	27	4.90	1.00	4.0	0.64	3.43	0.68	1.82	0.34	1.81	0.30	149.4	136.4	13.1
HD3-61	251.2	56.23	110	11.30	41	7.16	1.47	5.5	0.94	5.03	1.00	2.68	0.52	2.79	0.44	245.7	226.8	18.9
HD3-60	259.0	29.53	56	6.27	23	4.40	0.93	3.8	0.63	3.51	0.73	2.03	0.38	2.14	0.36	133.5	119.9	13.6
HD3-59	259.8	26.76	51	5.82	21	3.87	0.79	3.1	0.51	2.71	0.53	1.47	0.28	1.50	0.25	119.1	108.7	10.4
HD3-58	266.3	31.72	61	6.80	25	4.72	1.00	3.9	0.63	3.45	0.71	1.95	0.37	2.04	0.34	143.4	130.0	13.4
HD3-57	275.5	68.40	131	13.44	49	8.79	1.89	7.0	1.18	6.20	1.19	3.15	0.57	3.02	0.47	295.0	272.2	22.8
HD3-56	279.0	52.41	100	10.58	38	6.87	1.40	5.4	0.92	5.07	1.00	2.82	0.51	2.82	0.46	228.0	209.0	19.0
HD3-55	280.6	30.18	57	6.64	24	4.61	0.96	3.8	0.61	3.40	0.67	1.88	0.35	1.88	0.32	136.5	123.6	12.9
HD3-54	283.3	33.62	54	6.68	24	4.35	0.86	3.5	0.59	3.25	0.67	1.86	0.35	1.92	0.32	136.0	123.5	12.5
HD3-53	286.0	33.72	60	7.26	26	4.88	1.00	3.9	0.66	3.55	0.69	1.93	0.37	2.04	0.33	146.1	132.6	13.5
HD3-52	291.0	50.47	103	10.14	36	6.43	1.23	5.0	0.87	4.93	0.98	2.74	0.53	2.92	0.49	225.3	206.9	18.4
HD3-51	297.3	42.25	79	9.00	33	6.05	1.31	5.0	0.85	4.57	0.92	2.54	0.47	2.51	0.42	187.8	170.6	17.3
HD3-50	300.5	52.94	104	10.72	38	6.94	1.43	5.4	0.93	5.14	1.03	2.89	0.54	2.93	0.49	233.7	214.4	19.4
HD3-49	302.1	48.94	89	9.39	35	6.20	1.30	5.5	0.90	4.85	1.00	2.73	0.49	2.61	0.44	208.0	189.5	18.5
HD3-48	306.3	50.87	100	10.87	39	6.65	1.35	5.1	0.85	4.57	0.89	2.46	0.46	2.53	0.41	225.6	208.4	17.2
HD3-47	307.2	54.03	102	10.84	39	6.95	1.31	5.6	0.93	4.95	0.95	2.46	0.44	2.40	0.38	231.9	213.7	18.1
HD3-46	308.9	37.11	73	8.03	30	5.51	1.17	4.5	0.74	3.94	0.79	2.14	0.38	2.16	0.36	169.8	154.8	15.0
HD3-45	309.6	70.36	129	13.52	49	9.00	1.89	7.0	1.20	6.51	1.27	3.50	0.65	3.57	0.57	297.6	273.3	24.3
HD3-44	312.7	46.92	92	10.03	36	6.62	1.39	5.3	0.90	4.82	0.93	2.54	0.47	2.59	0.42	211.7	193.8	17.9
HD3-43	314.4	32.64	60	6.92	25	4.56	0.95	3.6	0.61	3.27	0.65	1.79	0.34	1.81	0.30	142.5	130.1	12.4
HD3-42	316.9	33.36	61	6.81	25	4.53	0.97	3.9	0.63	3.45	0.69	1.90	0.34	1.89	0.32	144.7	131.6	13.1
HD3-41	318.6	91.41	137	14.75	59	10.92	2.59	11.0	1.80	10.50	2.27	6.60	1.15	6.14	1.08	356.0	315.5	40.5
HD3-40	330.4	69.64	131	13.18	47	8.26	1.70	6.3	1.04	5.53	1.08	2.97	0.57	2.93	0.49	291.6	270.6	21.0
HD3-39	335.0	58.02	107	11.53	42	7.44	1.58	5.9	1.00	5.49	1.07	2.97	0.57	3.00	0.49	247.8	227.3	20.5
HD3-38	336.0	45.06	73	8.64	32	5.89	1.27	5.0	0.81	4.60	0.96	2.70	0.49	2.74	0.46	183.1	165.3	17.8
HD3-37	337.6	31.02	61	7.33	27	5.27	1.15	4.4	0.69	3.66	0.71	1.93	0.35	1.85	0.30	146.8	133.0	13.9
HD3-36	338.2	19.36	37	4.57	17	3.25	0.70	2.9	0.46	2.58	0.53	1.54	0.29	1.59	0.28	91.5	81.4	10.1
HD3-35	339.6	27.58	47	5.71	20	3.57	0.75	2.9	0.47	2.52	0.50	1.35	0.25	1.45	0.24	114.3	104.6	9.6
HD3-34	340.2	32.48	60	6.81	24	4.46	0.96	3.6	0.59	3.29	0.65	1.75	0.32	1.82	0.30	141.9	129.5	12.4
HD3-33	341.2	28.99	52	6.04	21	3.86	0.80	3.1	0.50	2.67	0.53	1.42	0.26	1.47	0.25	123.5	113.3	10.2
HD3-32	342.2	36.58	69	7.78	27	5.07	1.03	3.9	0.67	3.76	0.76	2.16	0.41	2.21	0.37	160.8	146.5	14.3
HD3-31	343.2	45.05	76	9.03	33	6.20	1.42	5.5	0.91	5.02	1.03	2.86	0.52	2.80	0.47	190.5	171.4	19.1
HD3-30	344.5	32.47	59	6.67	24	4.47	0.95	3.8	0.62	3.46	0.71	1.91	0.36	1.94	0.32	141.3	128.1	13.2
HD3-29	344.6	35.98	63	7.53	28	5.44	1.19	4.8	0.76	4.39	0.88	2.42	0.44	2.37	0.41	157.6	141.1	16.5

**Table 4:** Rare elements concentration and typical parameters of lake fine-grained clastic sediment in the Huadian Formation, Huadian Basin

LREE/HREE	(La/Yb) <sub>N</sub>	(Ce/Yb) <sub>N</sub>	(La/Sm) <sub>N</sub>	(Gd/Yb) <sub>N</sub>	$\delta\text{Eu}_N$	$\delta\text{Ce}_N$	Ce <sub>amon</sub>
12.5	14.7	10.5	5.8	1.5	0.68	0.99	-0.06
13.2	16.3	11.6	4.8	1.9	0.72	1.07	-0.02
11.9	12.5	13.7	5.0	1.5	0.72	1.13	0.01
10.5	11.3	14.2	4.9	1.4	0.70	1.04	-0.03
11.7	16.7	18.9	4.5	2.2	0.70	0.91	-0.09
10.8	11.2	12.6	4.9	1.3	0.66	1.06	-0.02
12.0	12.9	10.6	5.2	1.5	0.71	1.04	-0.03
10.6	11.7	11.0	5.2	1.3	0.65	0.97	-0.06
11.9	12.9	10.7	5.3	1.4	0.70	1.00	-0.04
11.0	14.1	10.1	5.3	1.6	0.72	0.87	-0.11
11.5	12.3	10.9	5.3	1.4	0.67	1.03	-0.03
9.1	9.6	18.3	4.2	1.4	0.67	1.03	-0.03
10.7	12.4	11.8	4.6	1.6	0.70	0.98	-0.05
12.2	13.6	12.9	4.9	1.6	0.69	1.05	-0.02
11.5	13.5	16.3	4.9	1.6	0.70	1.03	-0.03
8.2	8.2	13.3	4.0	1.3	0.72	1.00	-0.03
10.4	12.2	8.7	4.2	1.8	0.69	1.00	-0.03
12.0	13.6	13.3	4.9	1.6	0.71	1.05	-0.02
8.8	9.3	10.2	4.2	1.4	0.70	0.98	-0.04
10.5	12.0	7.2	4.4	1.7	0.69	0.98	-0.04
9.7	10.5	9.8	4.2	1.5	0.71	1.00	-0.04
11.9	15.3	14.4	4.9	1.9	0.74	1.04	-0.03
11.0	12.5	13.5	4.8	1.6	0.70	1.02	-0.03
9.6	10.8	9.0	4.1	1.6	0.70	0.97	-0.05
9.9	11.8	9.2	4.9	1.5	0.67	0.87	-0.10
9.8	11.1	9.8	4.4	1.5	0.70	0.92	-0.07
11.2	11.7	14.0	4.9	1.4	0.67	1.09	0.00
9.9	11.3	12.0	4.4	1.6	0.73	0.97	-0.05
11.1	12.2	14.0	4.8	1.5	0.71	1.05	-0.02
10.2	12.6	12.5	5.0	1.7	0.68	1.00	-0.05
12.1	13.6	12.1	4.8	1.6	0.71	1.02	-0.02
11.8	15.2	11.5	4.9	1.9	0.64	1.01	-0.04
10.3	11.6	10.3	4.2	1.7	0.72	1.02	-0.03
11.3	13.3	17.1	4.9	1.6	0.73	1.01	-0.05
10.8	12.2	12.4	4.5	1.6	0.72	1.02	-0.03
10.5	12.2	8.7	4.5	1.6	0.71	0.97	-0.05
10.0	11.9	9.0	4.6	1.7	0.70	0.98	-0.05
7.8	10.0	29.4	5.3	1.4	0.72	0.90	-0.13
12.9	16.0	14.0	5.3	1.7	0.72	1.04	-0.04
11.1	13.0	14.4	4.9	1.6	0.73	1.00	-0.05
9.3	11.1	13.1	4.8	1.5	0.72	0.89	-0.11
9.6	11.3	8.9	3.7	1.9	0.73	0.97	-0.04
8.0	8.2	7.6	3.7	1.5	0.70	0.94	-0.05
10.8	12.8	6.9	4.9	1.6	0.72	0.90	-0.08
10.5	12.0	8.7	4.6	1.6	0.72	0.98	-0.05
11.1	13.3	7.0	4.7	1.7	0.71	0.95	-0.06
10.3	11.2	10.6	4.5	1.4	0.71	0.98	-0.04
9.0	10.8	13.4	4.6	1.6	0.74	0.91	-0.09
9.7	11.3	9.3	4.6	1.6	0.70	0.97	-0.05
8.6	10.2	11.3	4.2	1.6	0.71	0.92	-0.08

## 5.1 Sedimentary provenance

Sediment compositions are characteristic of different assemblages of source rocks (Dickinson, 1985, 1988; McLennan et al., 1993). For example, REE abundances can be used to distinguish mafic and felsic sources. Generally, mafic rocks contain low LREE/HREE ratios and no Eu anomalies, whereas felsic rocks contain higher LREE/HREE ratios and a negative Eu anomaly (Charles et al., 2008; McLennan et al. 1993; Asedu et al., 2000). Hence, the observed LREE enrichment and negative Eu anomalies (Fig. 5a) indicate that fine-grained sediments in the Huadian Basin are derived from a felsic source. Correlations between total amounts of REEs and TOC contents and major element concentrations (Fig. 6) suggest that total amounts of REEs are mainly controlled by detrital minerals (Pyrite Member), aluminosilicate minerals (Oil Shale Member) or are enriched in coaly organic matter (Carbonaceous Shale Member).

Plots of La/Th versus Hf (Floyd and Leveridge, 1987), Co/Th versus La/Sc (Wronkiewicz and Condie, 1987) and La/Yb versus  $\Sigma\text{REE}$  (Allegre and Minster, 1978) are often used to analyze the source rocks. The Huadian samples in the three plots (Fig. 7a-c) indicate that they are mainly derived from felsic volcanic rocks and granites, mixed with small amount of mafic and sedimentary rocks. In the plot of Zr/Sc versus Th/Sc (McLennan et al., 1993), all samples may show a trend towards sediment recycling (Fig. 7d).

The basement units of the Huadian Basin are dominated by Paleozoic granite and minor sedimentary rocks of Paleozoic age exposed along the western and northern basin margins. South of the main fault, Mesozoic granite and Cretaceous sediments prevail (Fig. 1c). Meng et al. (2016) studied the percentage of sand layers in different units and concluded that sediment transport from northeastern and western directions prevailed during deposition of the Pyrite and Oil Shale members, but changed to southern directions during deposition of the Carbonaceous Shale Member. The geochemical and sedimentary analyses indicate a local provenance of the sediments of Huadian Formation, and that the changes of transport direction did not influence the overall geochemical composition of fine-grained sediments.

Sun (2010) studied the petrography of sandstones in the Huadian Basin. Typically, these sandstones comprise high contents of quartz (40-60 %), feldspars (15-30 %) and rock fragments (20-30 %). Most quartz grains are sub-angular to sub-rounded indicating limited transport distances. K-feldspar (including orthoclase and perthite) is significantly more abundant than plagioclase. The rock fragments are dominated by rhyolite and tuff. Sedimentary grains and phyllite could be observed occasionally (Sun,

2010). This shows that both, mudstones and sandstones reflect the same sediment source, dominated by felsic magmatic rocks and minor sediments.

Strong negative correlations between  $\text{Al}_2\text{O}_3$  and  $\text{SiO}_2$  for carbonate-free samples in the Pyrite and Carbonaceous Shale members (Fig. 3a, m) indicate that detrital quartz is a prominent  $\text{SiO}_2$  source for these members. In contrast, a positive correlation (Fig. 3g) suggests that clay minerals are the major  $\text{SiO}_2$  source for the mudstone-rich Oil Shale Member.

## 5.2 Weathering

Most elements, which are mobile during weathering (Ca, Na, K, P, Sr, Rb; Middelburg et al., 1988) are depleted in fine-grained sediments from the Huadian Basin relative to the UCC (Fig. 4a,b). The degree of chemical weathering can be estimated using the CIA (Nesbitt and Young, 1982) and CIA<sub>(molar)</sub> (Goldberg and Humayun, 2010), although chemical changes resulting from processes, such as diagenesis, provenance, physical weathering and sedimentary sorting, are not accounted for when using the CIA method. The average CIA

values for the Pyrite- (77), Oil Shale- (76) and Carbonaceous Shale (80) members (Table 2) reflect intermediate to strong chemical weathering. The A-CN-K ternary plot ( $A=\text{Al}_2\text{O}_3$ ;  $C=\text{CaO}$  (silicate fraction only);  $N=\text{Na}_2\text{O}$ ;  $K=\text{K}_2\text{O}$ ; Fig. 8a) shows that the samples from the Pyrite and Oil Shale members plot parallel to the A-CN line, indicating enrichment of  $\text{Al}_2\text{O}_3$  and leaching of  $\text{CaO}$  and  $\text{Na}_2\text{O}$ , while  $\text{K}_2\text{O}$  remains constant. Some samples from the Carbonaceous Shale Member plot closer to the A-K line and  $\text{Al}_2\text{O}_3$  apex, indicating leaching of  $\text{K}_2\text{O}$  and  $\text{Na}_2\text{O}$  (Fig. 8a). The CIA values of some samples from the Carbonaceous Shale Member exceed 85, indicating strong chemical weathering. This is further supported by negative correlations between Al and Na and K (Fig. 3q,r).

Similar results are obtained based on CIA(molar) values (Goldberg and Humayun, 2010; Sciscio and Bordy, 2016), which reach average values between 3.2 (Oil Shale Member) and 4.7 (Carbonaceous Shale Member) (Table 2).

## 5.3 Paleoclimate

Weathering is strongly related to climate, which also affect

Sample numbers	Depth /m	La	Ce	Pr	Nd	Sm	Eu	Gd	Tb	Dy	Ho	Er	Tm	Yb	Lu	$\Sigma\text{REE}$	$\Sigma\text{LREE}$	$\Sigma\text{HREE}$
HD3-28	344.7	44.91	79	9.30	34	6.28	1.35	5.1	0.86	4.54	0.92	2.45	0.46	2.40	0.39	192.4	175.2	17.1
HD3-27	344.8	37.01	69	8.38	31	5.77	1.19	4.4	0.73	3.81	0.72	1.91	0.36	1.92	0.31	166.2	152.1	14.2
HD3-26	345.3	35.04	57	7.38	26	4.94	1.06	4.0	0.67	3.67	0.73	2.07	0.40	2.16	0.36	146.3	132.2	14.1
HD3-25	345.8	41.38	84	10.03	38	7.15	1.51	5.5	0.87	4.31	0.80	2.07	0.38	2.04	0.33	198.0	181.8	16.3
HD3-24	346.8	60.99	124	13.28	47	8.37	1.68	6.1	1.00	5.10	0.97	2.47	0.46	2.56	0.41	274.7	255.7	19.0
HD3-23	348.0	78.14	132	15.29	56	10.14	2.09	7.7	1.28	6.83	1.27	3.47	0.64	3.47	0.56	318.8	293.5	25.3
HD3-22	352.6	67.18	112	12.54	44	7.63	1.42	5.8	0.94	5.08	0.97	2.62	0.49	2.63	0.42	263.9	244.9	18.9
HD3-21	357.1	57.50	109	11.76	43	7.63	1.64	5.9	1.00	5.43	1.06	2.98	0.57	3.04	0.49	250.9	230.4	20.5
HD3-20	357.7	50.78	100	11.16	42	8.22	1.88	7.0	1.17	6.15	1.16	2.97	0.52	2.73	0.43	236.6	214.5	22.2
HD3-19	359.8	53.46	100	11.01	39	6.92	1.35	5.3	0.84	4.35	0.81	2.18	0.41	2.22	0.36	229.0	212.5	16.4
HD3-18	369.5	13.04	25	3.16	11	2.13	0.46	2.0	0.29	1.65	0.34	1.00	0.18	1.07	0.20	62.1	55.3	6.8
HD3-17	370.5	29.74	56	6.46	23	4.27	0.88	3.6	0.60	3.42	0.69	1.99	0.38	2.18	0.37	133.2	120.0	13.2
<i>Pyrite Member</i>																		
HD3-16	373.9	89.51	167	19.30	71	13.12	2.81	10.2	1.71	8.83	1.61	4.22	0.76	4.03	0.65	394.4	362.4	32.0
HD3-15	385.9	73.23	138	14.51	52	9.21	1.93	7.0	1.18	6.20	1.19	3.23	0.60	3.27	0.53	311.7	288.6	23.2
HD3-14	388.2	71.38	125	13.41	50	9.09	2.00	7.8	1.28	6.93	1.36	3.67	0.64	3.47	0.56	296.2	270.5	25.7
HD3-13	392.2	71.48	134	14.02	51	9.49	2.06	7.8	1.33	7.01	1.36	3.70	0.66	3.60	0.59	308.3	282.2	26.1
HD3-12	397.2	59.17	115	12.38	45	8.13	1.68	6.3	1.05	5.65	1.09	2.91	0.55	3.09	0.50	262.8	241.6	21.2
HD3-11	472.1	50.74	95	10.26	36	6.32	1.27	4.8	0.81	4.41	0.86	2.39	0.46	2.50	0.41	215.9	199.3	16.7
HD3-10	478.7	62.35	106	11.98	44	7.98	1.71	6.4	1.06	5.66	1.09	2.96	0.54	2.97	0.49	254.9	233.7	21.1
HD3-09	484.8	51.51	92	10.64	38	6.95	1.47	5.5	0.92	4.86	0.92	2.50	0.47	2.50	0.40	219.1	201.0	18.1
HD3-08	490.9	67.35	128	13.93	51	9.37	2.00	7.5	1.30	6.97	1.34	3.71	0.69	3.73	0.60	297.6	271.8	25.9
HD3-07	496.5	70.11	132	14.27	52	9.57	1.98	7.6	1.29	6.96	1.33	3.59	0.67	3.67	0.59	306.1	280.4	25.7
HD3-06	503.7	47.83	92	9.84	35	6.63	1.41	5.4	0.94	5.36	1.06	3.02	0.57	3.10	0.51	212.2	192.3	20.0
HD3-05	507.0	52.71	106	11.57	43	7.86	1.71	6.7	1.11	5.89	1.16	3.19	0.57	2.99	0.50	244.8	222.7	22.1
HD3-04	516.2	34.16	63	7.30	26	4.74	1.01	3.9	0.63	3.49	0.68	1.92	0.36	1.93	0.32	150.1	136.9	13.2
HD3-03	520.2	37.12	63	6.82	22	3.65	0.71	2.9	0.48	2.68	0.56	1.62	0.31	1.76	0.29	143.8	133.2	10.6
HD3-02	536.1	84.27	152	16.54	60	10.94	2.38	8.6	1.45	7.63	1.42	3.88	0.71	3.77	0.61	354.7	326.6	28.1

N represents the chondrite-normalized values,  $(\text{La}/\text{Yb})_n$  is the ratio of  $\text{La}_n$  and  $\text{Yb}_n$ ,  $(\text{Ce}/\text{Yb})_n$  is the ratio of  $\text{Ce}_n$  and  $\text{Yb}_n$ ,  $(\text{La}/\text{Sm})_n$  is the ratio of  $\text{La}_n$  and  $\text{Sm}_n$ ,  $(\text{Gd}/\text{Yb})_n$  is the ratio

**Table 4:** continued

transportation and composition of the sediments. Climatic changes can also control lake-level variations and sediment supply rate. In the following, paleoclimatic changes are reconstructed using geochemistry and mineralogy.

### 5.3.1 Paleoclimate reconstruction by major elements and clay minerals

Weathering is strongly influenced by climatic factors. Therefore, CIA values also reflect paleoclimatic conditions. Weak weathering (CIA: 50-65) has been related to cold and dry climate. Intermediate (CIA: 65-85) and strong weathering (CIA: >85) have been related to warm and hot humid climates, respectively (Nesbitt and Yong, 1982; Bock et al., 1998; McLennan et al., 1993; see also Fig. 8a).

The CIA values in our study suggest that an overall subtropical warm and humid climate prevailed during deposition of the Huadian Formation. This interpretation is consistent with pollen data provided by Meng et al. (2016). These authors observed a dominance of angiosperm pollen, which include a high percentage of subtropical taxa such as Quercoidites,

Alnipollenites, Ulmpollenites and Tiliaepollenites. Using the Coexistence Approach (Mosbrugger and Utescher, 1997), Meng et al. (2016) reconstructed mean annual temperatures (MAT) and precipitation (MAP) in the order of 13.6-18.4°C and 887-1206 mm, respectively, which provide additional support for a subtropical warm and humid climate. Similar climatic conditions were reported by Quan et al. (2012) for different basins in northeast China.

Clay mineral assemblages also may reflect climatic changes in the source area (Singer, 1979, 1984; Deconinck et al., 2000; Chen et al., 2003; Meng et al., 2012a). In general, kaolinite is formed under humid climate by intense eluviations of feldspar, mica and pyroxene in acidic medium (Singer and Stoffers, 1980; Singer, 1984; Chamley, 1980; Lan, 1990; Tang et al., 2002). Authigenic smectite is formed under a dry-wet alternate climate (Dunoyer de Segonzac, 1970; Keller, 1970), whereas illite usually is formed under cool climate with low precipitation (Meunier, 1980). Therefore, kaolinite/clay minerals (K/C) and illite/clay minerals (I/C) ratios can be used to identify dry-wet changes of climate (Aplin, 1993). Vertical changes of K/C and I/C in the fine-grained sediments of the Huadian Basin are shown in Fig. 2a. Because of sampling limitations, we just discuss climate changes during deposition of the Oil Shale and Carbonaceous Shale members. Both, I/C and K/C ratios vary strongly in the Oil Shale Member. Moreover, smectite contents are higher in this member (Table 1). In the Carbonaceous Shale Member, K/C is significantly higher than I/C. These data, together with CIA and CIA(molar) values, which are higher in the Carbonaceous Shale Member than in other members of the Huadian Formation (Table 1; Fig. 8), may reflect a slight increase in temperature and humidity during deposition of the Carbonaceous Shale Member.

### 5.3.2 Paleoclimate reconstruction by trace elements

The climate sensitive Sr/Cu ratio (Lerman, 1989; Meng et al., 2012a; Liu et al., 1984) is plotted versus depth in Fig. 2c. Its vertical trend is uniform in the Pyrite and Carbonaceous Shale members but varies strongly in the Oil Shale Member. The result supports a climate with significant changes in humidity during deposition of the Oil Shale Member.

The above analysis shows that the climate changed during deposition of the Huadian Formation from a stable warm and humid climate (Pyrite Member), to a seasonal dry-wet climate (Oil Shale Member), to a stable warmer and more humid climate (Carbonaceous Shale Member). Probably, the precipitation changes were influenced by Eocene Asian monsoons (Quan et al., 2011, 2012). The stable warm and humid climate during deposition of the Carbonaceous Shale Member was beneficial for peat accumulation. The seasonal dry-wet climate during deposition of

LREE/HREE	(La/Yb) <sub>N</sub>	(Ce/Yb) <sub>N</sub>	(La/Sm) <sub>N</sub>	(Gd/Yb) <sub>N</sub>	$\delta\text{Eu}_N$	$\delta\text{Ce}_N$	Ce <sub>amon</sub>
10.2	12.6	11.5	4.5	1.7	0.73	0.93	-0.07
10.7	13.0	9.2	4.0	1.9	0.72	0.94	-0.05
9.4	10.9	10.3	4.5	1.5	0.73	0.86	-0.10
11.2	13.7	9.8	3.6	2.2	0.74	0.99	-0.03
13.4	16.1	12.2	4.6	1.9	0.72	1.05	-0.01
11.6	15.2	16.6	4.8	1.8	0.72	0.92	-0.09
12.9	17.2	12.6	5.5	1.8	0.65	0.93	-0.08
11.2	12.8	14.5	4.7	1.6	0.74	1.01	-0.04
9.7	12.5	13.1	3.9	2.1	0.76	1.01	-0.03
12.9	16.2	10.6	4.9	1.9	0.68	1.00	-0.04
8.2	8.2	5.1	3.8	1.5	0.67	0.95	-0.04
9.1	9.2	10.4	4.4	1.3	0.69	0.97	-0.05
11.3	15.0	19.3	4.3	2.0	0.74	0.97	-0.05
12.4	15.1	15.6	5.0	1.7	0.74	1.02	-0.04
10.5	13.9	16.6	4.9	1.8	0.73	0.97	-0.07
10.8	13.4	17.2	4.7	1.8	0.73	1.02	-0.04
11.4	12.9	14.8	4.6	1.6	0.72	1.03	-0.03
12.0	13.7	12.0	5.1	1.6	0.71	1.00	-0.04
11.1	14.2	14.2	4.9	1.7	0.73	0.93	-0.08
11.1	13.9	12.0	4.7	1.8	0.72	0.95	-0.06
10.5	12.2	17.8	4.5	1.6	0.73	1.01	-0.04
10.9	12.9	17.6	4.6	1.7	0.71	1.01	-0.04
9.6	10.4	14.8	4.5	1.4	0.72	1.02	-0.03
10.1	11.9	14.3	4.2	1.8	0.72	1.03	-0.02
10.4	11.9	9.2	4.5	1.6	0.72	0.97	-0.05
12.6	14.2	8.4	6.4	1.3	0.67	0.95	-0.08
11.6	15.1	18.0	4.8	1.8	0.75	0.98	-0.06

of Gd<sub>N</sub> and Yb<sub>N</sub>.  $\delta\text{Eu} = \text{Eu}_N / (\text{Sm}_N \times \text{Gd}_N)^{1/2}$ ,  $\delta\text{Ce} = \text{Ce}_N / (\text{La}_N \times \text{Pr}_N)^{1/2}$ , Ceanom = lg[3Ce<sub>N</sub>/(2La<sub>N</sub>+Nd<sub>N</sub>)].

the Oil Shale Member could have produced lake-level fluctuations, causing the accumulation of a high number of typically thin (1-2 m) oil shale layers.

## 5.4 Lake water environment

### 5.4.1 Salinity conditions

$\text{Sr/Ba}$ - Strontium (Sr) and barium (Ba) are alkaline earth metals with similar chemical properties. As Sr contents are higher in seawater,  $\text{Sr/Ba}$  ratios can be used to discriminate freshwater ( $\text{Sr/Ba} < 1$ ) and marine sediments ( $\text{Sr/Ba} > 1$ ) (Sun et al.,

1997).  $\text{Sr/Ba}$  ratios between 1.0 and 0.5 may indicate brackish-water. In lacustrine environments, a  $\text{Sr/Ba}$  ratio above 1.0 may indicate saline lake water under arid climate (Shi et al., 2003; Meng et al., 2012).

With only two exceptions (at 542.8 m and 516.2 m),  $\text{Sr/Ba}$  ratios in the Pyrite Member range from 0.21 to 0.63 (Fig. 2f), supporting a fresh-water environment. In the Oil Shale Member,  $\text{Sr/Ba}$  ratios vary between 0.22 and 1.29 (average 0.53), indicating alternating freshwater and saline conditions.  $\text{Sr/Ba}$  ratios of oil shale samples range from 0.33 to 1.09, with 74% of the samples showing ratios greater than 0.5. This may reflect that brackish water was beneficial for organic matter accumulation. High  $\text{Sr/Ba}$  ratios often correspond to high  $\text{Sr/Cu}$  values (see Fig. 2f), suggesting that salinity changes were caused by climatic changes. In the Carbonaceous Shale Member,  $\text{Sr/Ba}$  ratio range from 0.21 to 0.48, showing a fresh water environment.

$B$  and  $B/Ga$  - The chemical properties of boron (B) and gallium (Ga) differ significantly. B is a mobile element in water and its content increases with salinity (Deng and Qian, 1993). Ga is a more immobile element. Liu et al. (1984) have shown that the Ga contents are higher in continental fresh water mudstones (20-35 ppm) than in marine rocks (7-10 ppm). Therefore, B and  $B/Ga$  can be used as additional salinity proxies.

Generally, the content of B is below 60  $\mu\text{g/g}$  and  $B/Ga$  is lower than 3-3.3 in fresh-water lakes, whereas in salt water the B content and the  $B/Ga$  ratio exceed 100  $\mu\text{g/g}$  and 4.5-5.0, respectively (Deng and Qian, 1993; Wang et al., 1979).

The contents of B as well as the  $B/Ga$  ratios in the Pyrite (33.1-57.9  $\mu\text{g/g}$ ; 1.30-2.89) and Carbonaceous Shale members (27.4-63.7  $\mu\text{g/g}$ ; 0.97-2.91; Table 3), indicate a fresh water environment. Some higher concentrations and ratios are found in the Oil Shale Member (19.2-86.7  $\mu\text{g/g}$ ; 1.09-35.22; Table 3; Fig. 2d, g), reflecting temporal brackish water conditions.

Whereas both,  $\text{Sr/Ba}$  and  $B/Ga$  ratios, indicate temporarily enhanced salinity during deposition of the Oil Shale Member, organic geochemical proxies are less consistent (Strobl et al., 2015). According to these authors, TOC/S ratios generally above 2.8 indicating freshwater conditions, whereas relatively low methyltrimethyltridecylchroman (MTTC) ratios (0.23-0.66, Fig. 2h) indicate a salinity stratified, alkaline water column. However, the absence of gammacerane suggests that water column stratification originated without significant changes in bottom water salinity. The

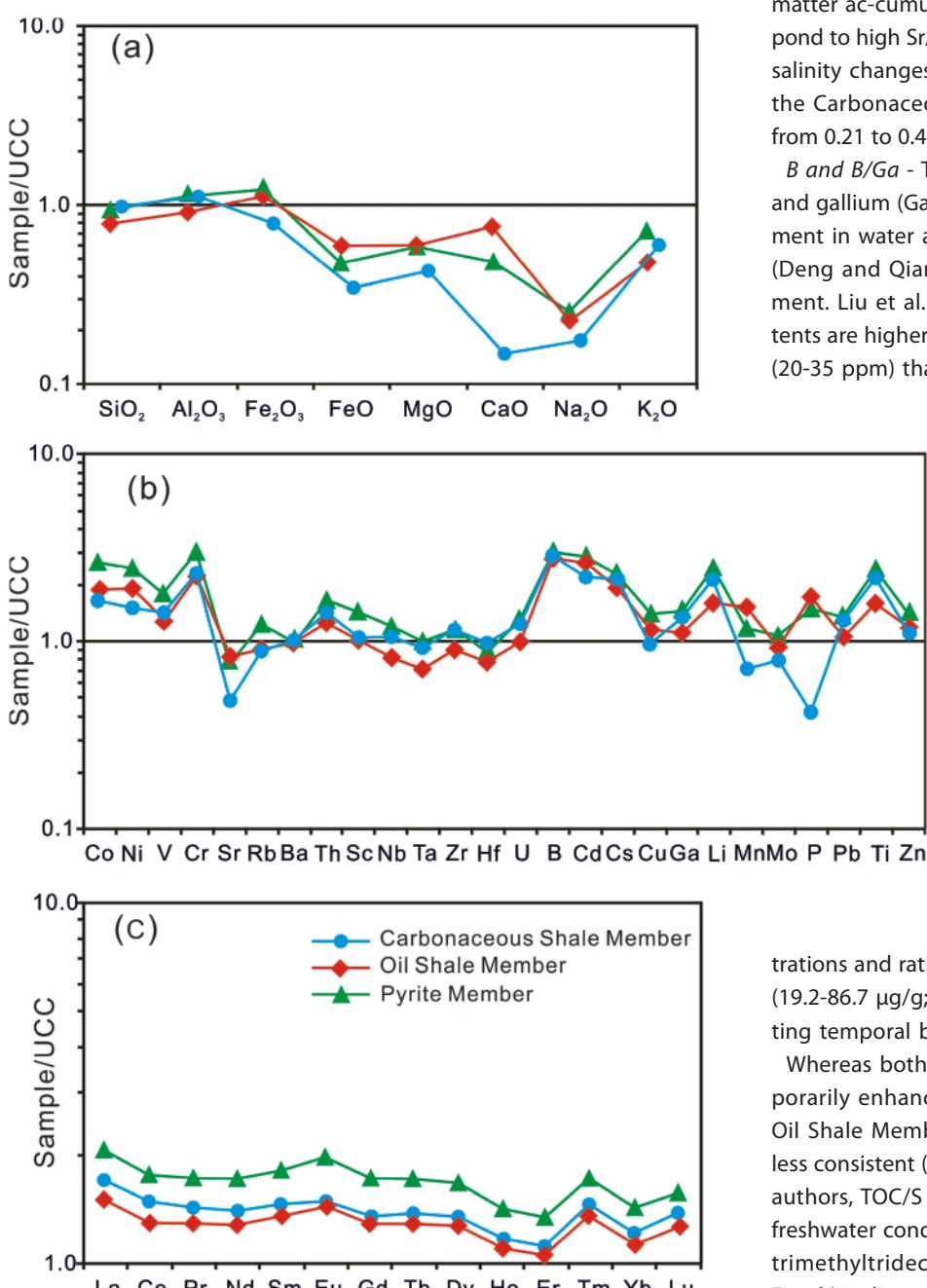


**Figure 4:** Major, trace and rare earth elements enrichment of fine-grained sediments in the Huadian Basin normalized to Upper Continental Crust (UCC; after Taylor and McLennan, 1985). (a) Major elements. (b) Trace elements. (c) Rare earth elements.

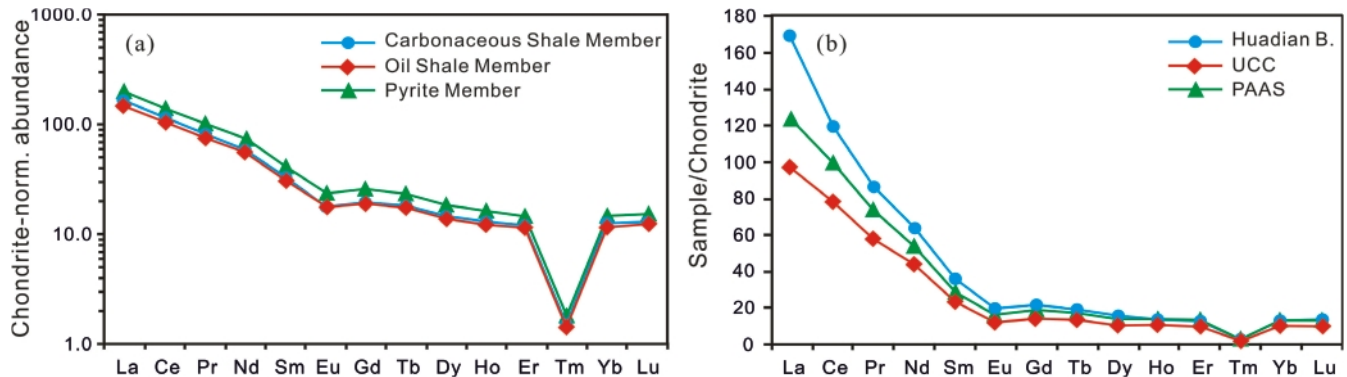


**Figure 5:** Chondrites-normalized REE plot (after Haskin and Haskin, 1966) for the fine-grain sediments in the Huadian Basin. (a) All units show LREE-enriched patterns and flat HREE patterns with slight negative Eu anomalies.(b) Comparison of chondrite-normalized REE patterns of average Huadian sediments with UCC and PAAS, the Huadian sediments plot closer to PAAS.

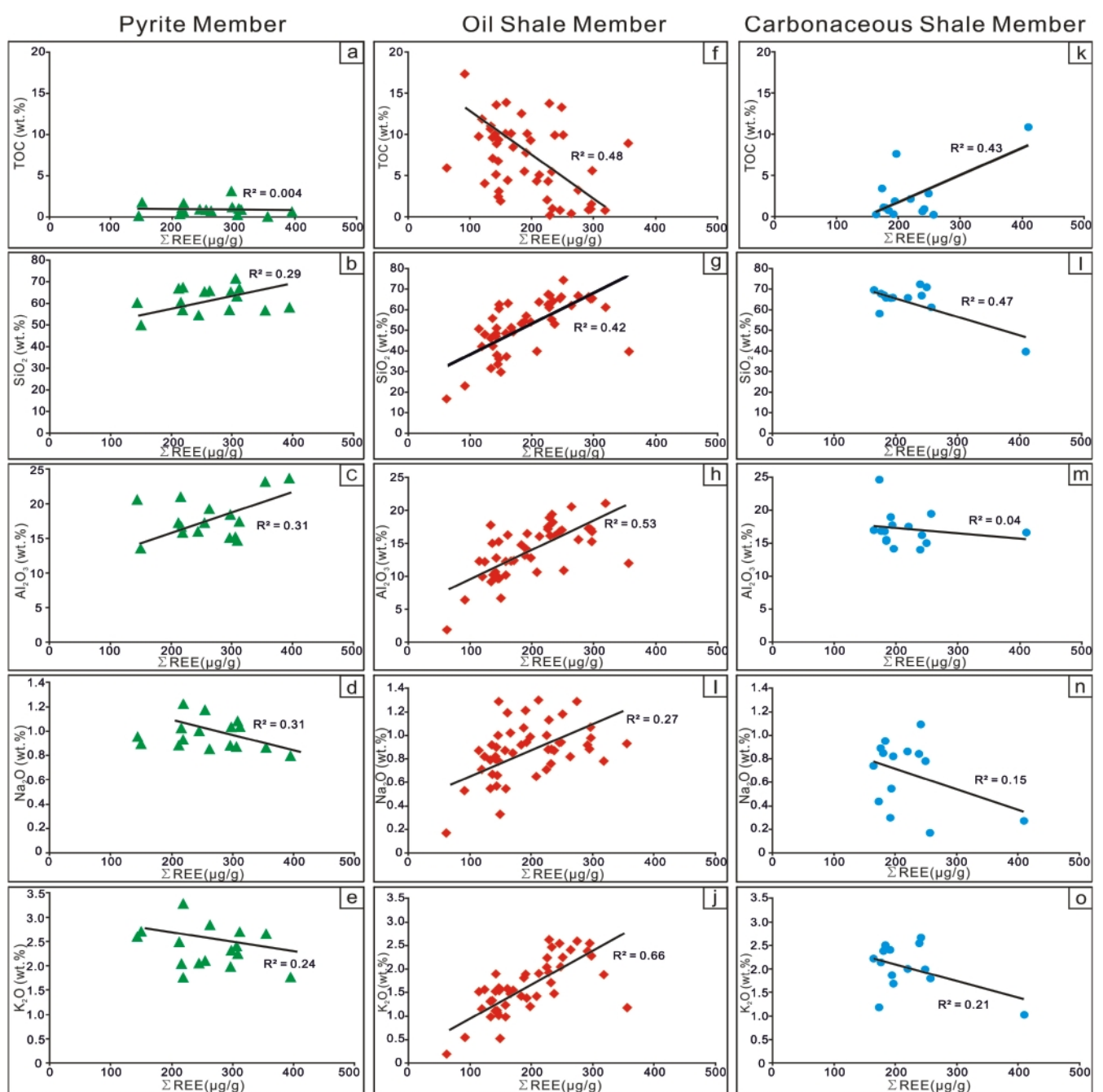


**Figure 6:** Correlations between  $\Sigma$ REE and TOC,  $\text{SiO}_2$ ,  $\text{Al}_2\text{O}_3$ ,  $\text{K}_2\text{O}$  and  $\text{Na}_2\text{O}$  of the fine-grained sediments in Huadian Basin.

presence of rhodophyta, described by Xie et al. (2014), even raises the possibility that deposition of some oil shale layers was influenced by marine flooding.

#### 5.4.2 Redox conditions

$V/(V+Ni)$ ,  $Ni/Co$ ,  $V/Cr$ ,  $Cu/Zn$  and  $(Cu+Mo)/Zn$ - The trace ele-

ments Mo, V, Ni and Mn are sensitive redox proxies (Anderson et al., 1989; Arthur et al., 1994; Morford and Emerson, 1999). Vanadium (V) is enriched in anoxic environment compared to nickel (Ni) (Lewan et al., 1982). Generally,  $V/(V+Ni)$  ratios greater than 0.60 reflect anoxia, ratios between 0.46 and 0.60 oxygen-depleted conditions, and ratios below 0.46 oxic environments (Wang, 2003; Teng et al. 2005).

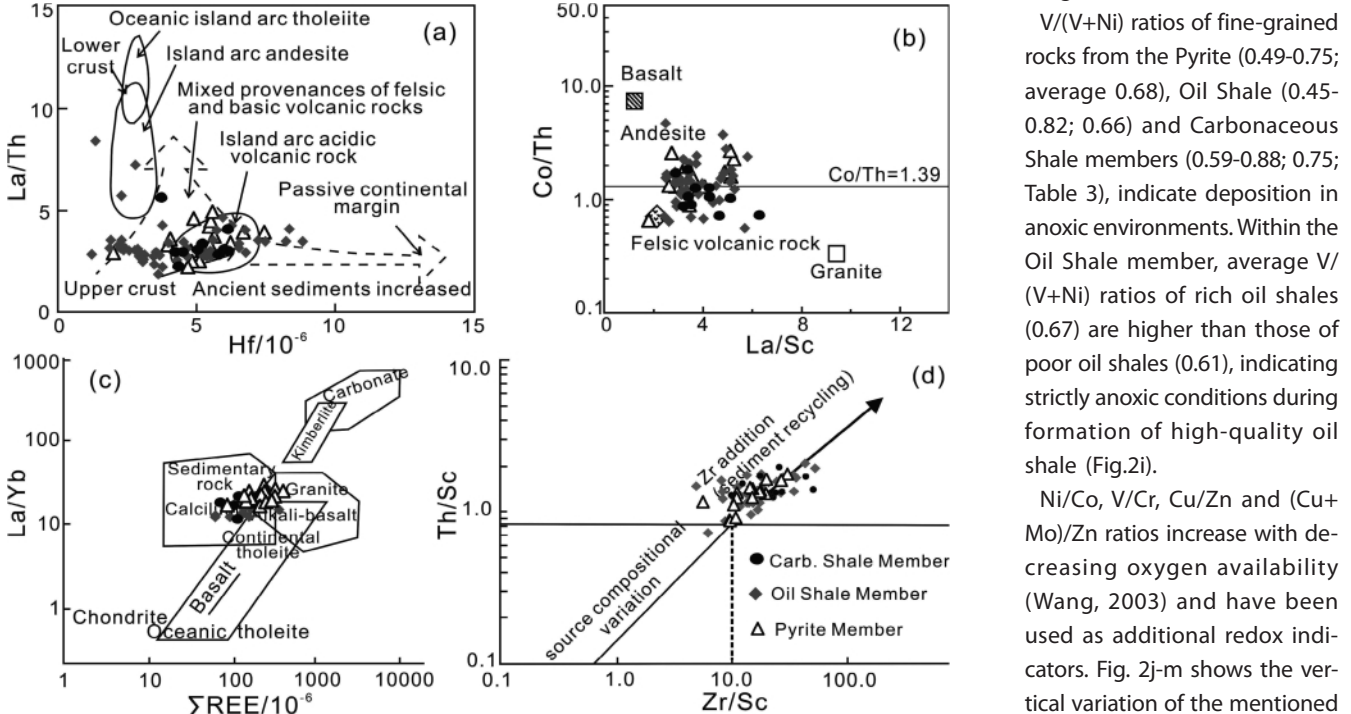


**Figure 7:** Plots to illustrate source rocks and sediment recycling (sources: a: Floyd and Leveridge, 1987; b: Wronkiewicz and Condé, 1987; d: McLennan et al. 1993). (a-c) show that the source rock of the fine-grained sediments are mainly derived from the felsic volcanic rocks and granites, mixed with minor amount of mafic and sedimentary rocks. (d) Plot of Th/Sc versus Zr/Sc indicating Zr addition due to sediment recycling.

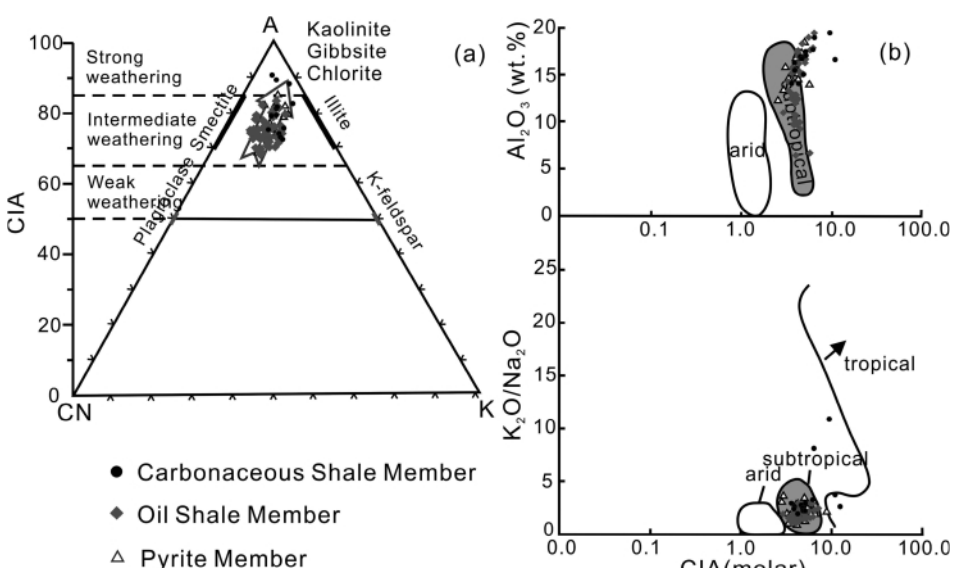


**Figure 8:** (a) Ternary plot of A-CN-K (in mole fraction), A =  $Al_2O_3$ , C =  $CaO$  (silicate fraction only), N =  $Na_2O$ , K =  $K_2O$ , F = total Fe as  $FeO$ , and M =  $MgO$  (after Nesbitt and Young, 1984, 1989). The position of samples from the Huadian basin indicates intermediate to strong chemical weathering. (b) Plots of CIA (molar) versus  $K_2O/Na_2O$  and  $Al_2O_3$  (after Goldberg and Humayun, 2010) suggesting that the Huadian Formation was deposited under subtropical conditions.

$V/(V+Ni)$  ratios of fine-grained rocks from the Pyrite (0.49-0.75; average 0.68), Oil Shale (0.45-0.82; 0.66) and Carbonaceous Shale members (0.59-0.88; 0.75; Table 3), indicate deposition in anoxic environments. Within the Oil Shale member, average  $V/(V+Ni)$  ratios of rich oil shales (0.67) are higher than those of poor oil shales (0.61), indicating strictly anoxic conditions during formation of high-quality oil shale (Fig. 2i).

$Ni/Co$ ,  $V/Cr$ ,  $Cu/Zn$  and  $(Cu+Mo)/Zn$  ratios increase with decreasing oxygen availability (Wang, 2003) and have been used as additional redox indicators. Fig. 2j-m shows the vertical variation of the mentioned element ratios. All ratios are relatively uniform in the Pyrite and Carbonaceous Shale members, but show some variability in the Oil Shale Member. As expected, average ratios in rich oil shales ( $Ni/Co$ : 2.49;  $V/Cr$ : 1.04;  $Cu/Zn$ : 0.37;  $(Cu+Mo)/Zn$ : 0.39) are slightly higher than in poor oil shale ( $Ni/Co$ : 2.31,  $V/Cr$ : 0.97,  $Cu/Zn$ : 0.34,  $(Cu+Mo)/Zn$ : 0.37; Table 3).

$Ce_{anom}$  - The cerium ( $Ce$ ) anomaly ( $Ceanom = \log[3Ce_n/(2La_n + Nd_n)]$ ; n represents chondrite normalized concentrations) has been introduced by Elderfield and Greaves (1982) and reflects the change of the ionic state of Ce as a function of the oxidation stage (Wilde et al., 1996). Generally, Ceanom above and below -0.1 indicates oxygen reduced and oxic environments, respectively (Elderfield and Greaves, 1982). The calculated Ceanom

values for fine-grained rocks in the Pyrite (-0.09 to -0.02; average -0.05), Oil Shale (-0.13 to -0.01; -0.05) and Carbonaceous Shale members (-0.11 to -0.02; -0.04; Table 4), reflect a strongly reducing environment.

The above trace element and REE proxies indicate that the fine-grained sediments from all members were deposited in oxygen-depleted environments. Oxygen depletion of lake water was relatively stable during deposition of the Pyrite and Carbonaceous Shale members, but more variable during deposition of the Oil Shale Member. They also show that strictly anoxic conditions were beneficial for the formation of high quality oil shale. These results are largely confirmed by biomarker proxies (Strobl et al., 2015). Pristane/phytane (Pr/Ph) ratios (Fig.2n; Strobl et al., 2015), a widely used redox parameter (Didyk et al., 1978) vary between 0.8 and 2.3 indicating dysaerobic to anaerobic conditions during deposition of fine-grained rocks in the Oil Shale Member. Very low amounts of arylisoprenoids show that permanent photic zone anoxia was not established (Strobl et al., 2015).

## 6. Conclusions

The Huadian Basin is an oil shale- and coal-bearing basin in northeast China. It is filled with the Eocene Huadian Formation, which includes from base to top the Pyrite, Oil Shale and Carbonaceous Shale members. The mineralogical and geochemical investigation revealed important insights into sediment provenance, different sedimentary processes, paleoclimate and depositional environment:

- Geochemical proxies, including concentrations of major, trace and rare earth elements, indicate that fine-grained sediments in the Huadian basin were derived from felsic volcanic rocks and granites, mixed with minor amounts of mafic volcanic rocks and sedimentary rocks. Zr/Sc and Th/Sc ratios confirm sediment recycling in the source region.
- Clay mineral assemblages are dominated by smectite and kaolinite indicating a very low diagenetic overprint. This result is supported by low thermal maturity of organic matter.
- Based on clay mineralogy and indices of chemical alteration, it is concluded that the climate changed during deposition of the Huadian Formation from a stable warm and humid climate (Pyrite Mbr.), to a seasonal dry-wet climate (Oil Shale Mbr.), to a stable warmer and more humid climate (Carbonaceous Shale Mbr.).
- The climatic conditions caused intermediate chemical weathering during deposition of the Pyrite and Oil Shale members and strong chemical weathering during deposition of the Carbonaceous Shale Member.
- Trace element ratios and Ceanom suggest that fine-grained rocks in the Huadian basin were deposited in anoxic freshwater environments. Fluctuations between fresh-water and brackish environments are restricted to the Oil Shale Member.
- The Eocene climatic change influenced lake level variations and water chemistry. Brackish water and strictly anoxic conditions were beneficial for the formation of high quality oil shale, whereas the warm and more humid climate domina-

ting during deposition of the Carbonaceous Shale Member favored peat accumulation.

## Acknowledgements

We would like to thank Royal Dutch Shell plc for generously providing the core HDN-glt-03 to Jilin University. The research project was financially supported by the National Natural Science Foundation of China (Grant No. 41302075), the Specialized Research Fund for the Doctoral Program of Higher Education of China (Grant No. 20110061120066), China Postdoctoral Science Foundation (Grant No. 2013M541291) and Science and technology development project of Jilin Province, China (Grant No. 20150622003JC). We thank two reviewers for valuable comments and suggestions.

## References

- Allegre, C.J. and Minster, J.F., 1978. Quantitative models of trace element behavior in magmatic processes. *Earth and Planetary Science Letters*, 38/1, 1-25. [https://doi.org/10.1016/0012-821X\(78\)90123-1](https://doi.org/10.1016/0012-821X(78)90123-1)
- Anderson, R.F., Fleisher, M.Q. and LeHuray, A.P., 1989. Concentration, oxidation state and particulate flux of uranium in the Black Sea. *Geochimica et Cosmochimica Acta*, 53, 2215-2224. [https://doi.org/10.1016/0016-7037\(89\)90345-1](https://doi.org/10.1016/0016-7037(89)90345-1)
- Aplin, A.C., 1993. The composition of authigenic clay minerals in recent sediments: links to the supply of unstable reactants. In: Manning, D.A.C., Hall, P.L., Hughes, C.R. (eds.), *Geochemistry of clay-pore fluid interactions*. Chapman & Hall, London, pp.81-106.
- Arthur, M.A. and Sageman, B.B., 1994. Marine black shales: depositional mechanism and environments of ancient deposits. *Annual Review of Earth and Planetary Science*, 22, 499-551. <https://doi.org/10.1146/annurev.ea.22.050194.002435>
- Asedu, D.K., Suzuki, S., Nogami, K. and Shibata, T., 2000. Geochemistry of Lower Cretaceous sediments, inner zone of southwest Japan: constraints on provenance and tectonic environment. *Geochemical Journal*, 34, 155-173. <http://doi.org/10.2343/geochemj.34.155>
- Bai, F.T., Guo, W., Lu, X.S., Liu, Y.M., Guo, M.Y., Li, Q. and Sun, Y.H., 2015. Kinetic study on the pyrolysis behavior of Huadian oil shale via non-isothermal thermogravimetric data. *Fuel*, 146, 111-118. <https://doi.org/10.1016/j.fuel.2014.12.073>
- Bai, Y.Y., Liu, Z.J., Sun, P.C., Liu, R., Hu, X.F., Zhao, H.Q. and Xu, Y.B., 2015. Rare earth and major element geochemistry of Eocene fine-grained sediments in oil shale-and coal-bearing layers of the Meihe Basin, Northeast China. *Journal of Asian Earth Sciences*, 97, 89-101. <https://doi.org/10.1016/j.jseas.2014.10.008>
- Bock, B., McLennan, S.M. and Hanson, G.N., 1998. Geochemistry and provenance of the Middle Ordovician Austin Glen Member (Normanskill Formation) and the Taconian orogeny in New England. *Sedimentology*, 45/4, 635-655. <https://doi.org/10.1046/j.1365-3091.1998.00168.x>

- Chamley, H., 1980. Clay sedimentation and paleoenvironment in the area of Daito Ridge (Northwest Philippine Sea) since the Early Eocene. In: Klein G., de Kobayashi K. V., et al., Initial Reports of the Deep Sea Drilling Project, 58, 683-690.
- Charles, K., Makenya, A.H.M. and Shukrani, M., 2008. Geochemistry of fine-grained clastic sedimentary rocks of the Neo-proterozoic Ikorongo Group, NE Tanzania: implications for provenance and source rock weathering. *Precambrian Research*, 164, 201-213. <https://doi.org/10.1016/j.precamres.2008.04.007>
- Chen, T., Wang, H., Zhang, Z.Q. and Wang, H.J., 2003. Clay minerals as indicators of paleoclimate. *Acta Petrologica et Mineralogica* 22/4, 416-420. [in Chinese with English abstract]
- Das, B.K. and Haake, B., 2003. Geochemistry of Rewalsar Lake sediment, Lesser Himalaya, India: implications for source-area weathering, provenance and tectonic setting. *Geosciences Journal*, 7, 299-312. <https://doi.org/10.1007/BF02919560>
- Deconinck, J.F., Blanc-Valleron, M.M., Rouchy, J.M., Camoin, G. and Badaut-Trauth, D., 2000. Palaeoenvironmental and diagenetic control of the mineralogy of Upper Cretaceous-Low Tertiary deposits of the Central Palaeo-Andean basin of Bolivia (Potosí area). *Sedimentary Geology*, 132, 263-278. [https://doi.org/10.1016/S0037-0738\(00\)00035-X](https://doi.org/10.1016/S0037-0738(00)00035-X)
- Deng, H.W. and Qian, K., 1993. Sedimentary geochemistry and environment analysis. LanZhou in China. Gansu Science and Technology Press, Gansu, China, pp.1-150. [in Chinese]
- Dickinson, W.R., 1985. Interpreting provenance relations from detrital modes of sandstones. In: Zuffa G.G. (ed.), Provenance of Arenites. Nato Science Series C: Mathematical and Physical Sciences, 48. Springer, Amsterdam, pp. 333-361.
- Dickinson, W.R., 1988. Provenance and sediment dispersal in relation to paleotectonics and paleogeography of sedimentary basins. In: Kleinspehn, K.L. and Paola, C. (eds.), New perspectives in basin analysis. Springer, New York, pp. 3-25.
- Didyk, B.M., Simoneit, B.R.T., Brassell, S.C. and Eglington, G., 1978. Organic geochemical indicators of palaeoenvironmental conditions of sedimentation. *Nature*, 272, 216-222. <https://doi.org/10.1038/272216a0>
- Dunoyer de Segonzac, G., 1970. The transformation of clay minerals during diagenesis and low grade metamorphism: a review. *Sedimentology*, 15, 281-346. <https://doi.org/10.1111/j.1365-3091.1970.tb02190.x>
- Elderfield, H. and Greaves, M.J., 1982. The rare earth elements in seawater. *Nature*, 296 (5854), 214-219. <https://doi.org/10.1038/296214a0>
- Fedo, C.M., Nesbitt, H.W. and Young, G.M., 1995. Unraveling the effects of potassium metasomatism in sedimentary rocks and paleosols, with implications for paleoweathering conditions and provenance. *Geology*, 23, 921-924. [https://doi.org/10.1130/0091-7613\(1995\)023<0921:UTEOPM>2.3.CO;2](https://doi.org/10.1130/0091-7613(1995)023<0921:UTEOPM>2.3.CO;2)
- Floyd, P.A. and Leveridge, B.E., 1987. Tectonic environment of the Devonian Gramscatho basin, south Cornwall: framework mode and geochemical evidence from turbiditic sandstones. *Journal of the Geological Society*, 144/4, 531-542. <https://doi.org/10.1144/gsjgs.144.4.0531>
- Goldberg, K. and Humayun, M., 2010. The applicability of the chemical index of alteration as a paleoclimatic indicator: An example from the Permian of the Paraná Basin, Brazil. *Palaeogeography, Palaeoclimatology, Palaeoecology*, 293, 175-183. <https://doi.org/10.1016/j.palaeo.2010.05.015>
- Jiang, H.F., Song, L.H., Cheng, Z.Q., Chen, J., Zhang, L., Zhang, M.Y., Hu, M.J., Li, J.N. and Li, J.F., 2015. Influence of pyrolysis condition and transition metal salt on the product yield and characterization via Huadian oil shale pyrolysis. *Journal of Analytical and Applied Pyrolysis*, 112, 230-236. <https://doi.org/10.1016/j.jaap.2015.01.020>
- Jin, Z. D., Li, F.C., Cao, J.J., Wang, S.M. and Yu, J.M., 2006. Geochemistry of Daihai Lake sediments, Inner Mongolia, north China: Implications for provenance, sedimentary sorting and catchment weathering. *Geomorphology*, 80, 147-163. <https://doi.org/10.1016/j.geomorph.2006.02.006>
- Johnsson, M.J., 1993. The system controlling the composition of clastic sediments. *Geological Society of America Special Papers*, 284, 1-20. <https://dx.doi.org/10.1130/SPE284-p1>
- Keller, W. D., 1970. Environmental aspects of clay minerals. *Journal of Sedimentary Petrology*, 40, 788-859.
- Lan, X.H., 1990. Clay minerals as an index of paleoclimate. *Geological science and technology information*, 9/4, 30-35. [in Chinese with English abstract]
- Laird, K.R., Cumming, B.F., Wunsam, S., Rusak, J.A., Oglesby, R.J., Fritz, S.C. and Leavitt, P.R., 2003. Lake sediments record large-scale shifts in moisture regimes across the northern prairies of North America during the past two millennia. *Proceedings of the National Academy of Sciences*, 100, 2483-2488. <https://doi.org/10.1073/pnas.0530193100>
- Last, W.M. and Smol, J.P. (eds.), 2001. *Tracking Environmental Change Using Lake Sediments*. Kluwer Academic Publishers, Dordrecht, Netherlands, pp.107-135.
- Lewan, M.D. and Maynard, J.B., 1982. Factors controlling enrichment of vanadium and nickel in the Bitumen of organic sedimentary rocks. *Geochimica et Cosmochimica Acta*, 46, 2541-2560. [https://doi.org/10.1016/0016-7037\(82\)90377-5](https://doi.org/10.1016/0016-7037(82)90377-5)
- Lerman, A., 1989. Lakes Chemistry and Geology Physics, Translated by Wang Sumin et al., Geological Press, Beijing, China, pp. 1-65.
- Li, D.F., Chen, H.Y., Zhang, L., Fralick, P., Hollings, P., Mi, M., Lu, W.J., Han, J.S., Wang, C.M. and Fang, J., 2017. Geochemistry of fine-grained clastic rocks in the Mesoproterozoic Kawabulake Group: implications for provenance and the tectonic model of the Eastern Tianshan, Xinjiang, NW China. *International Journal of Earth Sciences*, 106, 115-129. <https://doi.org/10.1007/s00531-016-1304-5>
- Liu, J.H., Wu, Z.X., Yu, S. and Jia, D.H., 2005. Paleocene trace element geochemistry and its geological significance in Lishui sag. China offshore oil and gas 17/1, 8-11. [in Chinese with English abstract]
- Liu, Y.J., Cao, L.M., Li, Z.L., Wang, H.N., Chu, T.Q. and Zhang, J. R., 1984. *Elementary geochemistry*. Science Press, Beijing, China, pp.1-80.
- Manchester, S.R., Chen, Z., Geng, B. and Tao, J., 2005. Middle

- Eocene flora of Huadian, Jilin Province, Northeast China. *Acta Palaeobotanica*, 45/1, 3-26.
- McLennan, S.M., 1989. Rare earth elements in sedimentary rocks: influence of provenance and sedimentary processes. *Reviews in Mineralogy and Geochemistry*, 21, 170-199.
- McLennan, S.M., 2001. Relationships between the trace element composition of sedimentary rocks and upper continental crust. *Geochemistry, Geophysics, Geosystems*, 2/4, 1525-2027. <https://doi.org/10.1029/2000GC000109>
- McLennan, S.M., Hemming, S., McDaniel, D.K. and Hanson, G. N., 1993. Geochemical approaches to sedimentation, provenance, and tectonics. In: Johnsson, M. J., and Basu, A. (eds.), *Processes Controlling the Composition of Clastic Sediments*. Geological Society of America Special Paper 284, 21-40.
- Meng, Q.T., Liu, Z.J., Bruch, A.A., Liu, R. and Hu, F., 2012a. Palaeoclimatic evolution during Eocene and its influence on oil shale mineralization, Fushun Basin, China. *Journal of Asian Earth Sciences*, 45, 95-105. <https://doi.org/10.1016/j.jseaes.2011.09.021>
- Meng, Q.T., Liu, Z.J., Hu, F., Sun, P.C., Zhou, R.J. and Zhen, Z., 2012b. Productivity of Eocene ancient lake and enrichment mechanism of organic matter in Huadian Basin. *Journal of China University of Petroleum*, 36/5, 38-44. [in Chinese with English abstract].
- Meng, Q.T., Liu, Z.J., Liu, R., Sun, P.C., Hu, F. and Zhang, J., 2011. Comparison on the characteristics of biomarkers of oil shale between Huadian Formation in Huadian Basin and Green River Formation in Uinta Basin of Western United States. *Journal of Jilin University (Earth Science Edition)*, 41(2), 391-399. [in Chinese with English abstract]
- Meng, Q.T., Liu, Z.J., Sun, P.C., Jia, J.L. and Hu, F., 2016. Sequence Stratigraphy and Sedimentary Environment of the Eocene Huadian Formation in the Huadian Basin (NE China): Implications for Oil Shale Distribution. *Russian Journal of Pacific Geology (Russian Edition)*, 35/6, 81-101.
- Meunier, A., 1980. Lesménismes de l'altération des granites et le rôle des microsystèmes. Etude des arenas du massif granitique de Parthenay (Deux-Sèvres) Mémoire de la Société Géologique de France, 150-160.
- Middelburg, J.J., Weijden, C.H. and Woittiez, J.R.W., 1988. Chemical processes affecting the mobility of major, minor and trace elements during weathering of granitic rocks. *Chemical Geology*, 68/3-4, 253-273. [https://doi.org/10.1016/0009-2541\(88\)90025-3](https://doi.org/10.1016/0009-2541(88)90025-3)
- Morford, J.I. and Emerson, S., 1999. The geochemistry of redox sensitive trace metals in sediments. *Cosmochim Acta*, 63, 1735-1750. [https://doi.org/10.1016/S0016-7037\(99\)00126-X](https://doi.org/10.1016/S0016-7037(99)00126-X)
- Mosbrugger, V. and Utescher, T., 1997. The coexistence approach-a method for quantitative reconstructions of Tertiary terrestrial palaeoclimate data using plant fossils. *Palaeogeography, Paleoclimatology, Paleoecology*, 134, 61-86. [https://doi.org/10.1016/S0031-0182\(96\)00154-X](https://doi.org/10.1016/S0031-0182(96)00154-X)
- Nesbitt, H.W. and Young, G.M., 1982. Early Proterozoic climates and plate motions inferred from major element chemistry of lutites. *Nature*, 299, 715-717. <https://doi.org/10.1038/299715a0>
- Quan, C., Liu, Y.S. and Utescher, T., 2011. Paleogene evolution of precipitation in northeast China supporting the middle Eocene intensification of the East Asian monsoon. *Palaeos*, 26, 743-753. <https://doi.org/10.2110/palo.2011.p11-019>
- Quan, C., Liu, Y.S. and Utescher, T., 2012. Paleogene temperature gradient, seasonal variation and climate evolution of northeast China. *Palaeogeography, Paleoclimatology, Paleoecology*, 313-314, 150-163. <https://doi.org/10.1016/j.palaeo.2011.10.016>
- Ren, L., Xia, D.H., Xu, Y.B., Guo, M.R., Sun, H. and Liu, X., 2015. Research on Pyrolysis Mechanism of Huadian Oil Shale. *Energy Procedia*, 66, 13-16. <https://doi.org/10.1016/j.egypro.2015.02.007>
- Rietveld, H. M., 1969. A profile refinement method for nuclear and magnetic structures. *Journal of Applied Crystallography*, 2, 65-71. <https://doi.org/10.1107/S0021889869006558>
- Sciscio, L. and Bordy, E.M., 2016. Palaeoclimatic conditions in the Late Triassic-Early Jurassic of southern Africa: A geochemical assessment of the Elliot Formation. *Journal of African Earth Sciences*, 119, 102-119. <https://doi.org/10.1016/j.jafrearsci.2016.03.014>
- Shi, J.A., Guo, X.L., Wang, Q., Yan, N.Z. and Wang, J.X., 2003. Geochemistry of REE in QH1 Sediments of Qinghai Lake since Late Holocene and Its Paleoclimatic Significance. *Journal of Lake Sciences*, 15/1, 28-33. [in Chinese with English abstract]
- Singer, A., 1979. The paleoclimatic interpretation of clay minerals in soil and weathering-a review. *Earth-Science Review*, 15, 303-326. [https://doi.org/10.1016/0012-8252\(80\)90113-0](https://doi.org/10.1016/0012-8252(80)90113-0)
- Singer, A., 1984. The paleoclimatic interpretation of clay minerals in sediment-a review. *Earth-Science Review*, 21, 251-293. [https://doi.org/10.1016/0012-8252\(84\)90055-2](https://doi.org/10.1016/0012-8252(84)90055-2)
- Singer, A. and Stoffers, P., 1980. Clay-mineral diagenesis in two East African lake sediments. *Clay Minerals*, 15, 291-307.
- Strobl, S.A.I., Sachsenhofer, R.F., Bechtel, A., Meng, Q.T. and Sun, P.C., 2015. Deposition of coal and oil shale in NE China: The Eocene Huadian Basin compared to the coeval Fushun Basin. *Marine and Petroleum Geology*, 64, 347-362. <https://doi.org/10.1016/j.marpetgeo.2015.03.014>
- Sun, X.M., Wang, S.Q., Wang, Y.D., Du, J.Y. and Xu, Q.W., 2010. The structural feature and evolutionary series in the northern segment of Tancheng-Lujiang fault zone. *Acta Petrologica Sinica*, 26/1, 165-176. [in Chinese with English abstract]
- Sun, P.C., 2010. Research on sedimentary characteristics of Huadian Formation of Paleogene in Huadian Basin. Master Thesis, Jilin University, Changchun, China, pp. 14-22.
- Sun, P.C., Liu, Z.J., Meng, Q.T., Liu, R., Jia, J.L. and Hu, X.F., 2011. Effect of the basin-fill features on oil shale formation in Paleogene, Huadian Basin. *Journal of China Coal Society*, 36/7, 1110-1116. [in Chinese with English abstract]
- Sun, P.C., Sachsenhofer, R.F., Liu, Z.J., Strobl, S.A.I., Meng, Q.T., Liu, R. and Zhen, Z., 2013. Organic matter accumulation in the oil shale- and coal-bearing Huadian Basin (Eocene; NE China). *International Journal of Coal Geology*, 105, 1-15. <https://doi.org/10.1016/j.coal.2012.11.009>

- Sun, Y.H., Bai, F.T., Lu, X.S., Jia, C.X., Wang, Q., Guo, M.Y., Li, Q. and Guo, W., 2015. Kinetic study of Huadian oil shale combustion using a multi-stage parallel reaction model. *Energy*, 82, 705-713. <https://doi.org/10.1016/j.energy.2015.01.080>
- Sun, Z.C., Yang, F., Zhang, Z.H., Li, S.J., Li, D.M., Peng, L.C., Zeng, X.L., Xu, Y.L., Mao, S.Z. and Wang, Q., 1997. Seolmentirry Environments and Hydrocarbon Generation of Cenoaoic Salified Lakes in China. Petroleum Industry Press, Beijing, China, pp. 35-120.
- Tang, Y.J., Jia, J.Y. and Xie, X.D., 2002. Environment significance of clay minerals. *Earth Science Frontiers*, 9/2, 337-344. [in Chinese with English abstract]
- Taylor, J. C., 1991. Computer programs for standardless quantitative analysis of minerals using the full powder diffraction profile. *Powder Diffraction*, 6, 2-9. <https://doi.org/10.1017/S0885715600016778>
- Taylor, S.R. and McLennan, S.M., 1985. The Continental Crust: Its Composition and Evolution. Blackwell, London, 184 pp.
- Teng, G.E., Liu, W.H., Xu, Y.C. and Chen, J.F., 2005. Correlative study on parameters of inorganic geochemistry and hydrocarbon source rocks formative environment. *Advances in Earth Sciences* 20(2), 193-200 (in Chinese with English abstract).
- Volkman, J.K., Zhang, Z.R., Xie, X.M., Qin, J.Z. and Borjigin, T., 2015. Biomarker evidence for Botryococcus and a methane cycle in the Eocene Huadian oil shale, NE China. *Organic Geochemistry*, 78, 121-134. <https://doi.org/10.1016/j.orggeochem.2014.11.002>
- Wang, Y.L., Liu, Z.J., Jing, H.L., Zhang, H.L. and Zhang, J., 2005. Sedimentary characteristics of oil shale deposit of the Huadian Formation of Paleogene in Huadian Basin. *Journal of Jilin University (Earth Science Edition)*, 35/6, 720-731. [in Chinese with English abstract]
- Wang, Y.Y., Guo, W.Y. and Zhang, G.D., 1979. Application of some geochemical indicators in determining of sedimentary environment of the Funing Group (Paleogene), Jin-Hu Depression, Kiangsu Province. *Journal of Tongji University* (2), 51-60. [in Chinese with English abstract]
- Wang, Z.M., 2003. Geochemical indicators for diagnosing anoxic sedimentary environment. *Acta Geologica Gansu*, 12/2, 55-58. [in Chinese with English abstract]
- Weltje, G.J. and Von Eynatten, H., 2004. Quantitative provenance analysis of sediments: review and outlook. *Sedimentary Geology*, 171, 1-4. <https://doi.org/10.1016/j.sedgeo.2004.05.007>
- Wilde, P., Quinby-Hunt, M.S. and Erdtmann, B.D., 1996. The whole-rock cerium anomaly: a potential indicator of eustatic sea-level changes in shales of anoxic facies. *Sedimentary Geology*, 101, 43-53. [https://doi.org/10.1016/0037-0738\(95\)00020-8](https://doi.org/10.1016/0037-0738(95)00020-8)
- Wronkiewicz, D.J. and Condie, K.C., 1987. Geochemistry of Archean shales from the Witwatersrand Supergroup, South Africa: source-area weathering and provenance. *Geochim. Cosmochim. Acta*, 51/9, 2401-2416. [https://doi.org/10.1016/0016-7037\(87\)90293-6](https://doi.org/10.1016/0016-7037(87)90293-6)
- Xie, X.M., Volkman, J.K., Qin, J.Z., Borjigin, T., Bian, L.Z. and Zhen, L.J., 2014. Petrology and hydrocarbon potential of microalgal and macroalgal dominated oil shales from the Eocene Huadian Formation, NE China. *International Journal of Coal Geology*, 124, 36-47. <https://doi.org/10.1016/j.coal.2013.12.013>
- Zhang, Z.R., Volkman, J. K., Greenwood, P. F., Hu, W., Qin, J.Z., Borjigin, T., Zhai, C.B. and Liu, W.X., 2014. Flash pyrolysis of kerogens from algal rich oil shales from the Eocene Huadian Formation, NE China. *Organic Geochemistry*, 76, 167-172. <https://doi.org/10.1016/j.orggeochem.2014.08.004>
- Zhou, J.J. and Sun, J.R., 1985. The Late of Early Eocene fishes were found in Huadian Basin, Jilin Province in China. *Vertebrata Palasiatica*, 23/2, 170. [in Chinese]

Received: 22 June 2017

Accepted: 25 October 2017

QingTao MENG<sup>1,2\*)</sup>, Reinhard F. SACHSENHOFER<sup>2</sup>, ZhaoJun LIU<sup>1</sup>, PingChang SUN<sup>1</sup>, Fei HU<sup>1</sup>, RenJie ZHOU<sup>3</sup> & KeBing WANG<sup>1</sup>

<sup>1</sup> College of Earth Sciences, Jilin University, 130061 Changchun, China;

<sup>2</sup> Department Applied Geosciences and Geophysics, Montanuniversität, 8700 Leoben, Austria;

<sup>3</sup> School of Earth and Environmental Sciences, The University of Queensland, St Lucia, 4072 QLD, Australia;

<sup>\*)</sup> Corresponding author, mengqt@jlu.edu.cn